DATE DUE	DATE DUE	DATE DUE
[illegible]		

LIGHT MEDIUM SEPARATION OF HIGH DENSITY POLYETHYLENE AND POLYPROPYLENE IN A HYDROCYCLONE

By

David Charles Carlson

A THESIS

Submitted to
Michigan State University
in partial fulfillment of the requirements
for the degree of

MASTER OF SCIENCE

Department of Chemical Engineering

1995

ABSTRACT

LIGHT MEDIUM SEPARATION OF HIGH DENSITY POLYETHYLENE AND POLYPROPYLENE IN A HYDROCYCLONE

By

David Charles Carlson

Experiments were conducted to study the use of hydrocyclones to separate high density polyethylene (HDPE) and polypropylene (PP) from glass microbubbles and water. The size distribution of the microbubbles is much smaller than the size of the two plastic constituents. Experiments show that the recovery of HDPE in the underflow stream increases as the effective density of the feed stream decreases below 900 kg/m^3. The purity of the underflow stream, as measured by the mass ratio of HDPE/PP, remains above 9 for feed densities above 800 kg/m^3. The high microbubble loading in the feed stream is attributed to the concomitant separation of the low density microbubbles in the flow field. The critical factors which control the HDPE/PP separation performance include the concentration of microbubbles in the underflow stream, the geometry of the hydrocyclone, and the flow split ratio. The recovery coefficient E_1 for HDPE can be correlated with ρ_F/ρ_{50}, where ρ_F is the density of the feed stream and ρ_{50} is an intrinsic cut-density of the separator.

To my wife and my parents...

Acknowledgments

I wish to thank Dr. Charles A. Petty and Dr. Syed K. Ali for their guidance in this research, and the undergraduate employees of the hydrocyclone research lab, especially John Burke, who assisted me with the experiments. Funding for this research was provided by the American Plastics Council, the Department of Energy Innovative Concepts Program, the Michigan State University Foundation, the Michigan Materials and Processing Institute, and the State of Michigan Research Excellence Fund. Technical assistance and materials were provided by Robert Hill of 3M, Gerald Kelton and Mark Hoyack of Krebs Engineers, Paul Marsh of Michigan Polymer Reclaim, and PlastiPak.

TABLE OF CONTENTS

LIST OF TABLES

LIST OF FIGURES

Notation

$\lvert \Delta P \rvert$	Absolute value of the pressure drop over the hydrocyclone
$\langle u_\theta \rangle$	Average tangential velocity
b	Parameter used to fit an exponential curve to HDPE yield data
C_P	Pressure loss coefficient
DMH	Dense medium hydrocyclone
E_1	Recovery of HDPE in the underflow stream
E_2	Recovery of PP in the overflow stream
HDPE	High Density Polyethylene
K	Constant relating pressure drop to flow rate
LMH	Light medium hydrocyclone
M_{1x}	HDPE stream purity coefficient in stream x
M_{2x}	PP stream purity coefficient in stream x
n	constant relating pressure drop to flowrate
N	Hydrodynamic parameter relating tangential velocity to location in the hydrocyclone
$\mathcal{P}$	Power (watts)
PP	Polypropylene

Q_X	Volumetric flowrate of stream x
r	Radial distance from vortex axis
Re	Reynolds number
S	Split ratio
TRCZ	Toroidal Recirculation Zone
v	Bulk feed velocity to the hydrocyclone
w_{ix}	Mass fraction of constituent i in stream x
y_{ix}	Volume fraction of constituent i in stream x

Greek

Φ_F	Density ratio
α	Major cone angle
β	Underflow cone angle
ε_1	Overflow purity coefficient
ε_2	Underflow purity coefficient
l	Diameter of a particle
ρ	Density
ρ_{50}	Feed density at which 50 % of the HDPE reports to the UF

Subscripts

1	HDPE
2	PP
3	Microbubble

4	Water
F	Feed
H	Hydrocyclone
O	Overflow
U	Underflow

CHAPTER 1

INTRODUCTION

1.1 Motivation

The rapid increase in the use of thermoplastics have led to many improvements and advancements in the automotive and packaging industries. These materials offer the advantages of relatively low weight/cost and durability over traditional materials such as paper and steel. However, these same properties make thermoplastics a problem when their useful life cycle has ended inasmuch as they comprise a disproportionate volume of landfill space when compared to other materials such as glass and steel.

Like many other materials presently going to landfills, thermoplastics have the option of being recycled and reused. Table 1 shows that the rate of thermoplastic recycling is growing rapidly. With this expansion, it has become increasingly important to obtain clean feed stocks from this resource. This study is concerned with the removal of contaminate thermoplastics from HDPE. Most thermoplastics are heavier than water and are easily removed from HDPE, which has a density lower than that of water. PP, however, also has a density lower than water and is difficult to separate from HDPE.

Table 1: Growth in Plastic Packaging Recycling (APC, 1993)

Resin Type	Percent Change from 1990 to 1991
PET	29.2
HDPE	75.1
PVC	6.7
LDPE/LLDPE	10.4
PP	1200
PS	85.3

Unfortunately, the presence of PP in the recycle waste stream may affect the physical properties of the reclaimed HDPE. For instance, PP has a much lower izod impact strength than HDPE (see Table 2). Also, PP may have a different color than HDPE as is the case with a milk jug and its PP cap. Even in small amounts, the PP may change the hue of the reclaimed HDPE, making it more difficult to obtain a consistent product (Carlson et al., 1993). The demand for uncolored material is much greater than the demand for a colored product. In 1993, the estimated amounts of recycled HDPE in the United States were 240 million pounds for natural HDPE and 125 million pounds for the colored material. This represented approximately 3% of the virgin HDPE sales for that same year (Carlson et al., 1993). The national goal for recycling HDPE is 10% of virgin sales, so there is tremendous opportunity for separating PP from HDPE.

1.2 Background

There are several different methods being evaluated for microsorting mixed streams of thermoplastics. These include float/sink technology, optical techniques, chemical solvation, and hydrocyclones. Table 3 briefly summarizes the advantages and disadvantages of the listed methods. The simplest method for separating PP and HDPE is the float/sink process in which PP is the light component and HDPE is the heavy component. This type of process may employ either a homogeneous fluid or a fine suspension with an effective density

Table 2: Properties of HDPE and PP

Resin	Density* (kg/m^3)	Glass Transition Temp.* (°C)	Fracture at Cryogenic Temp.* (°C)	Brittle Temp.* (°C)	Izod Impact Strength* (ft-lb/in)
HDPE	941 - 965	-122	Difficult to Fracture	~ -150	0.8 - 14
PP	900 - 910	-20	Fractures	< 20	0.4 - 0.6

* Modern Plastic Encyclopedia '95, Mid-Nov. 1993
* Braton. N.R., Cryogenic Recycling and Processing, 1980

Table 3: Options for Microsorting Mixed Thermoplastics

Separation Method	Components	Advantages	Disadvantages
Float/Sink	Super Critical Fluids, Microbubbles, Organic Liquids	Density is easily controlled	Large volumes; Long residence times
Optical Techniques		Unique polymer signature; work with filled materials	High Tech, Expensive
Chemical Solvation	Xylene	Work with wide range of polymers; can achieve 100% purity	Harmful chemicals; high waste treatment costs
Hydrocyclones	Same as Float/Sink	Compact; retrofit; low capital cost	Cannot achieve complete separation

in-between HDPE and PP (Atland et al.,1994; Nugent, 1991). The same materials which are used in float/sink operations can also be used in a hydrocyclone. The hydrocyclone offers the advantages of short residence times, easy adaptability into existing plants, and relatively low capital cost. However, complete separation does not usually occur in hydrocyclones.

Figure 1 illustrates the concept of separating HDPE and PP in a hydrocyclone using a suspension of glass microbubbles and water. Separation occurs because the size distribution of the microbubbles is much smaller than the size of the two plastics and makes the suspension appear as an effective medium. In this environment, PP migrates towards the axis of the flow field and is removed with the overflow stream. The HDPE migrates towards the outer portion of the flow field and is removed in the underflow. This practical application of an effective light medium in a hydrocyclone, albeit challenging, has much commercial potential.

The use of suspensions to separate materials of different specific gravities is not new. The first commercial use of a heavy-medium separation in the U.S. was in 1936 by the American Zinc Company for separating ZnS and limestone (American Cyanamid, 1951). The dense medium hydrocyclone (DMH) for coal beneficiation was developed by the Dutch State Mines in the late 1930's (Driessen, 1939). The

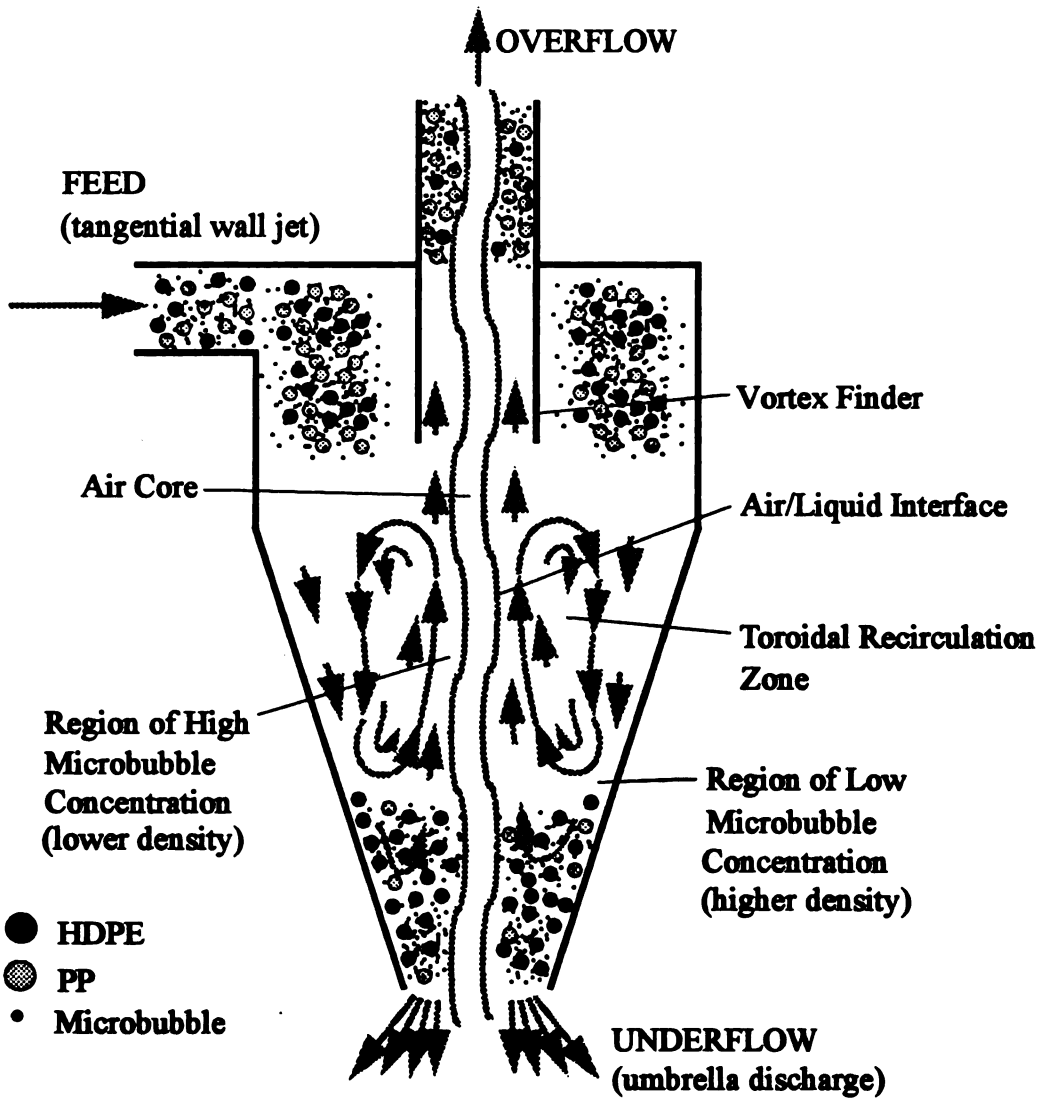

Figure 1: Separation Concept

further development of technology for dense media separations continues as an active area of research. Coal and shale mixtures with particle sizes between 1-6 mm are easily separated in hydrocyclones using magnetite suspensions. Presently, hydrocyclone technology is being investigated to separate coal particles which are finer than 150 μm (Miller, 1991). The analog of the dense medium hydrocyclone for a light medium separation will be designated LMH.

1.3 Objectives

The goal of this study is to explore the separation performance of a commercial hydrocyclone for separating HDPE and PP using a fine suspension of glass microbubbles. The split ratio, inlet density, flow rate, and cone angle significantly affect the separation performance of a DMH, so these same factors should also be important for a LMH operation.

1.4 Methodology

This thesis examines the separation of HDPE and PP using an effective light medium of glass microbubbles and water in a hydrocyclone. The plastics used were obtained from PlastiPak, Inc. (Plymouth, MI) and the microbubbles were obtained from 3M (St. Paul, MN). The plastics were shredded to obtain a size appropriate for testing. A dense medium hydrocyclone was supplied by Krebs Engineers (Menlo Park, CA) for testing the LMH concept. Initial tests were

conducted to determine if the available flow loop in the hydrocyclone laboratory could handle the thermoplastic/glass microbubble/water mixture and to determine if PP and HDPE could be separated. This study explores in more detail the earlier proof of concept study of Petty et al. (1993).

Chapter 2 summarizes the physical properties of the glass microbubbles, PP, and HDPE used in this study. The light medium flow circuit, test hydrocyclones, experimental procedures, and the theoretical basis for evaluating the separation performance are also developed in Chapter 2. In Chapter 3, the experimental results are presented and then discussed in Chapter 4. The conclusions and engineering significance of the results are presented in Chapter 5. A material balance flow sheet for the use of the LMH concept to a specific HDPE/PP process stream illustrates the potential of the proposed separation strategy. Chapter 6 identifies further research and development needed to commercialize the LMH technology.

CHAPTER 2

EXPERIMENTAL DESIGN

2.1 Glass Microbubbles

Selection of Light Medium

The choice of an appropriate suspending medium for an LMH is critical. Although there are many options for controlling the specific gravity for DMH, there are few naturally occurring substances available with densities lower than water. Table 4 lists possible materials for LMH. These options are: organic liquids, air, fly ash, and hollow glass spheres (microbubbles). This sections describes the advantages and disadvantages of these materials, and why glass microbubbles were chosen for this study.

Organic liquids, such as ethanol and methanol, offer the advantage of a completely stable medium in that the suspending medium is a homogeneous continuous phase. This greatly simplifies the control of the separation because the density of the continuous phase is uniform throughout the system, and can be tightly controlled by mixing two fluids. However, the physical properties of HDPE may be affected by the presence of an organic liquid. For instance, the organic liquids may absorb into the HDPE, swell the polymer and, thereby, alter the physical

Table 4: Options for Lowering the Density of the Continuous Phase

Material	Advantages	Disadvantages
Organic Liquids	Easily controlled density; uniform density	May interact chemically with plastics; high recovery costs
Air Bubbles	Low cost; no need for recovery	Possible problems with stability, coalescence
Fly Ash	Great abundance; little or no cost	Small amount of floaters; dependent on feed coal stock
Microbubbles	No interactions with thermoplastics; easily recovered	Cost; losses due to breakage; unstable medium

properties (Encyclopedia of Polymers, 1988). For this reason, organic liquids were not chosen as the method for lowering the density of water between HDPE and PP.

Another option for lowering the density of the continuous phase is sparged air. By passing an air stream through a porous medium, small air bubbles can be formed which have a suitable size distribution for light medium cycloning. An air sparged hydrocyclone is a very attractive prospect because of the relatively low cost of generating the bubbles, and because the air would not have to be recovered. Also, unlike an organic liquid, the air bubbles would not interact chemically with the polymers, or change the physical properties of the HDPE and PP. The air sparged hydrocyclone is not without its own difficulties. There may be possible stability problems with the air bubbles. Although it may be possible to obtain a suitable feed size distribution, the turbulent environment within a hydrocyclone may break the air bubbles or allow them to coalesce forming a distribution quite different from that of the feed. In either case, the resulting size distribution may not be suitable for this particular application.

Fly ash was studied as another option for lowering the density of the continuous phase. Fly ash is a waste material from coal burning power plants which, if not captured, would fly out the top of the smokestack. The composition of the fly ash

depends on the source of the coal and the operating conditions of the burner. A portion of fly ash has a density which is less than that of water, so it was conjectured that this material may also be suitable for light medium cycloning. Also, since this is a waste product, the fly ash would be available at a low cost.

Samples of fly ash were obtained from the MSU Power Plant and the Lansing Board of Water and Light. The samples were tested for particle size distribution and density distribution (floaters/sinkers). The particle size was determined to be approximately 30 μm and the average density was estimated to be about 2000 kg/m^3 for both samples. It was noted that there were floaters in each sample, but the amounts were too small for any analysis. Although fly ash may be an economically appealing option, the samples examined were inadequate for this study.

Glass microbubbles were chosen as the suspended material for the light medium hydrocyclone. The microbubbles are comprised of a glass shell with an air core, and are commercially available from the 3M Company. The microbubbles were chosen because they offer the advantages of low density and small size. Also, the glass microbubbles do not interact with either HDPE or PP, and they are easily removed and recovered from the thermoplastics. However, the microbubbles used in this investigation have two disadvantages: (1) they quickly migrate to the vortex

core and are removed with the overflow stream (see Figure 1); and, (2) they break in high shear flows. These issues will be addressed in detail later in this thesis.

Density of Microbubbles

The density of microbubbles is an important parameter in the light medium separation. The density determines the concentration of microbubbles necessary to produce a given inlet density and affects the stability of the water/microbubble suspension. The average density of the glass microbubbles was determined using the following procedure. A small amount of glass microbubbles of known mass was placed into a graduated cylinder partially filled with a known volume and mass of water. The cylinder was covered and agitated to suspend the microbubbles. The total volume of the suspension was quickly determined before a significant portion of the microbubbles came out of suspension, thus skewing the reading. Knowing the mass and volume of the microbubbles allowed the density to be calculated. The average density of the K20 distribution was determined to be 210 kg/m^3 and that of the K46 distribution to be 440 kg/m^3. The manufacturer's values for these distributions are 200 kg/m^3 and 460 kg/m^3, respectively. Although the density of a microbubble is inversely related to its diameter (Ali et al., 1992), this study did not attempt to determine a mathematical expression for the density as a function of diameter.

Microbubble Size Distributions

The size distribution was determined via light scattering using a Malvern MasterSizer X. A dilute suspension of glass microbubbles was placed in a small flow cell and pumped through the MasterSizer. The MasterSizer requires the refractive indices of the continuous and dispersed phases, and the absorption of the dispersed phase. A refractive index of 1.54 and an absorption of 0.01 were used for the glass microbubbles, and a refractive index of 1.33 was used for the water. The MasterSizer was programmed to take 50 sweeps of the light intensity within its cavity, and then calculate a size distribution from these readings. This procedure was repeated three times and the results were averaged. A mean size of 52 μm and 32 μm was determined for the K20 and K46 microbubble distributions, respectively. The manufacturer's numbers for these distributions are 62 μm and 44 μm, respectively. The cumulative distributions for these microbubbles are shown in Figure 2. The actual data from the Malvern MasterSizer are presented in Tables B.2 and B.3.

The size of the microbubbles is a major factor controlling the migration of the microbubbles towards the core of the vortex. For a particle Reynolds number less than 0.1, Stokes' law provides a good approximation for the drift velocity (Svarovsky, 1984):

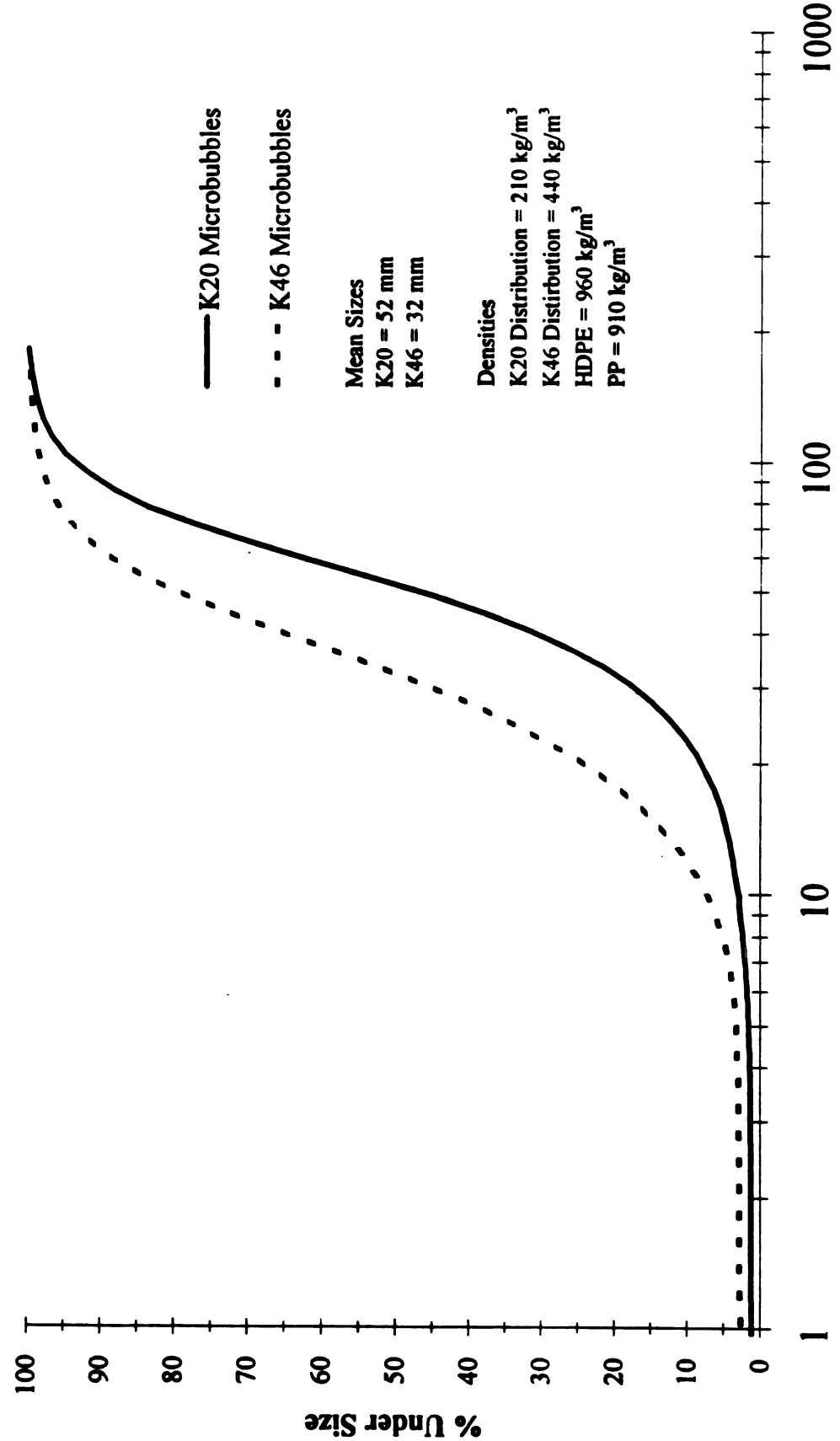

Figure 2: Size Distributions of Glass Microbubbles

$$u_D = \frac{\ell^2 (\rho_C - \rho_B)}{18\mu_C} \frac{<u_\theta>^2}{r} \qquad (1)$$

In the above equation, the following definitions apply:

u_D = drift velocity of the particle
ℓ = microbubble diameter
ρ_C = density of the carrier fluid (water)
ρ_B = density of the microbubble
μ_C = viscosity of the carrier fluid (water)
r = radial distance from the vortex axis (see Figure 1)
$<u_\theta>$ = swirl component of the mean velocity

For ℓ = 32 μm, ρ_C = 1000 kg/m^3, ρ_B = 440 kg/m^3, μ_C/ρ_C = 0.01 cm^2/s, $<u_\theta>$ = 2 m/s, and r = 5 cm, the drift velocity given by Eq. 1 is approximately 0.25 cm/s for $Re = \ell\rho_C u_D/\mu_C = 0.08$. As the microbubble migrates towards the core (i.e. $r \rightarrow 0$), the acceleration of the particle, $<u_\theta>^2/r$, may increase from 8g near the wall to 80g near the air core (see Figure 1). The magnitude of this effect obviously depends on the internal flow patterns and the behavior of $<u_\theta>$.

Clearly Eq. (1) shows that reducing the size of the microbubbles will significantly decrease the drift velocity and may, thereby, increase the stability of the suspension. For the two microbubble products used in this investigation, the ratio of drift velocities for the mean particle size is

$$\frac{u_D(K20)}{u_D(K46)} = \frac{[\ell^2(\rho_C - \rho_B)]_{K20}}{[\ell^2(\rho_C - \rho_B)]_{K46}} = \left(\frac{52}{32}\right)^2 \left(\frac{0.79}{0.56}\right) = 3.7.$$

2.2 High Density Polyethylene and Polypropylene

Size Distributions of HDPE and PP

The HDPE and PP were obtained from PlastiPak, Inc. in Plymouth, Michigan. The HDPE was received in the form of detergent bottles with PP being the cap. These sources had not been in contact with any chemicals and were considered to be pure thermoplastics. Due to losses while conducting the experiments, these plastics were augmented with more HDPE and PP. Both the HDPE and PP from this secondary source were unpigmented and could not be distinguished from each other after shredding so the materials had to be run separately. The sizes of HDPE and PP were reduced using a shredder which is housed in the School of Packaging. Shredding is distinguished from grinding in that shredding entails the slicing of a material with a sharp edge, while grinding causes size reduction by impacting a material with a blunt device and actually shattering the piece into smaller fractions.

The size distributions of HDPE and PP were determined on a mass basis using an automated shaker and standardized sieves of known size. The sieves were placed in descending order of size into the shaker and then the plastics were allowed to separate for thirty minutes. The weight of thermoplastic on each tray was determined, giving the cumulative size distributions for HDPE and PP shown in Figure 3. The sizes of the sieves and data for determining the cumulative size

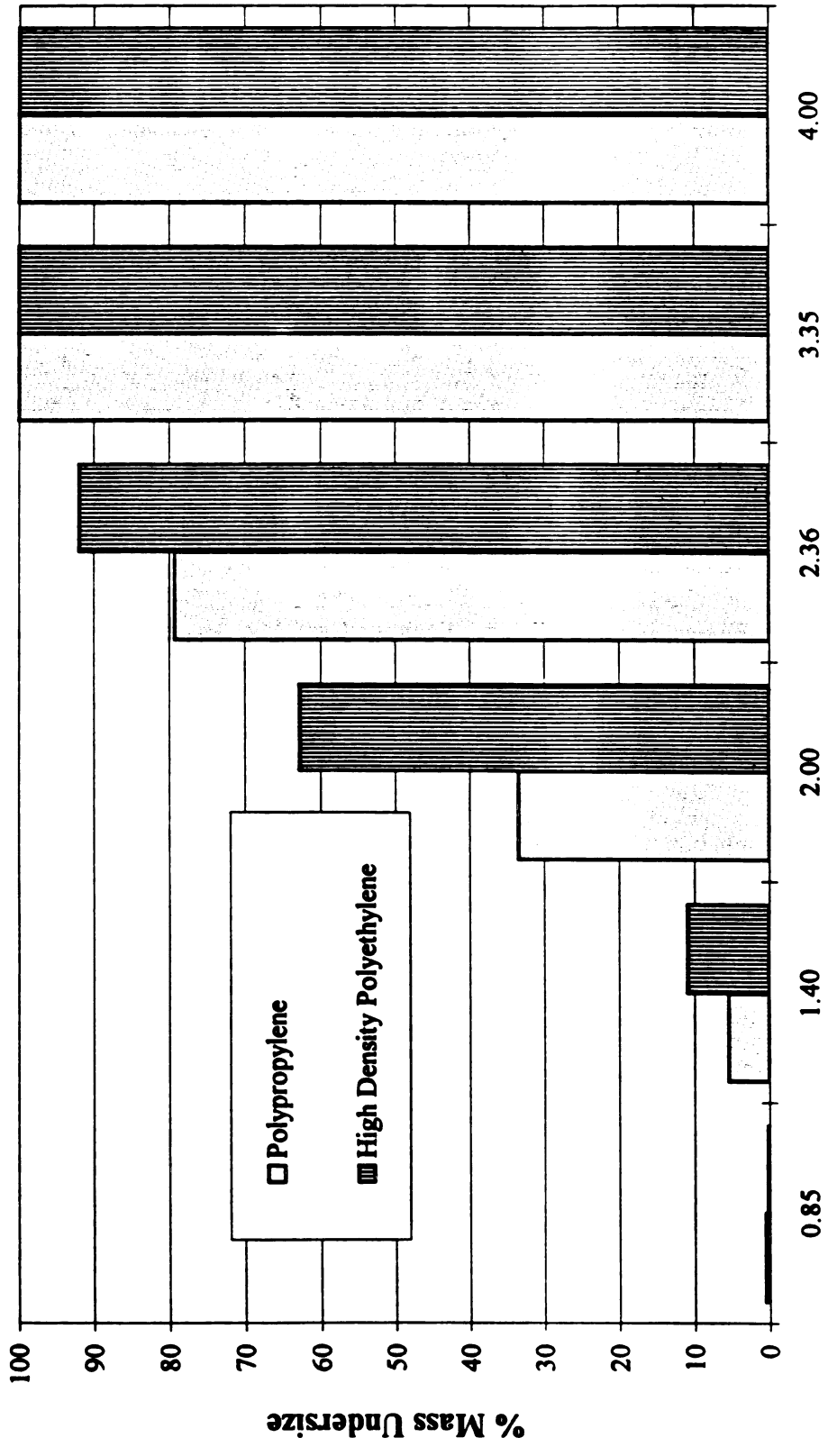

Figure 3: Size Distributions of PP and HDPE

distributions are shown in Table C.1. Figure 3 shows that HDPE and PP have approximately the same size distribution and that 90 % of the material has a screen size between 1 mm and 3 mm. These values are much larger than the average sizes of the microbubbles (52 and 32 μm) and allows the suspension to act as an effective medium. Figure 4 shows the microbubbles compared to the HDPE and PP.

Density of HDPE and PP

The densities and density difference between two materials is important for separation in a hydrocyclone (see Eq. (1)). These factors influence the choice of medium and the density control of the effective continuous phase (microbubble and water). The larger the density difference, the less stringent the control of the feed density. The densities of both HDPE and PP are less than that of water (≈ 1000 kg/m^3). As shown in Table 2 (see p. 4), HDPE and PP have density ranges which are distinct from each other.

The densities of HDPE and PP were determined using a gravimetric method. A known weight of thermoplastic was placed in a graduated cylinder partially filled with a known volume and weight of methanol. The volume change was determined and the density of the material was calculated. Using this method, the

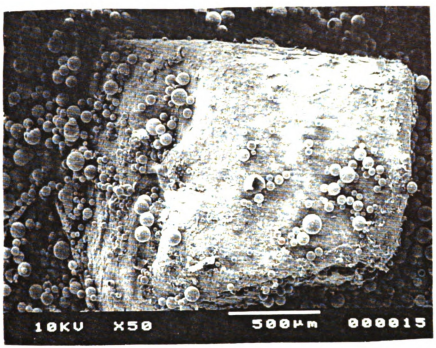

PP

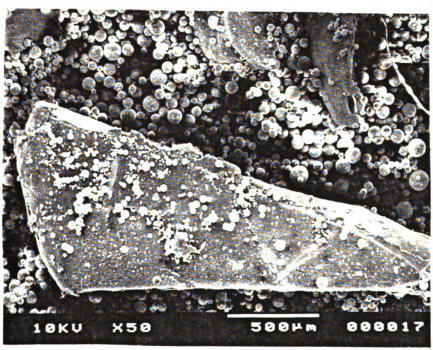

HDPE

Figure 4: SEM Micrographs of HDPE and PP with Microbubbles

density of HDPE was determined to be 960 kg/m^3, and that of PP to be 910 kg/m^3. These numbers are within the range of tabulated values shown in Table 2.

2.3 Test Hydrocyclones

A commercial 100 mm dense media hydrocyclone was used for this study. The hydrocyclone is constructed of a metal outer shell and a polyurethane inner lining. The polyurethane protects the metal shell from the abrasive conditions of dense media separations and is easily replaced. The hydrocyclone is comprised of four major sections with different interchangeable parts for the cone and underflow. This modular design allows for a wide range of geometries to be studied. Figures 5 and 6 show the hydrocyclone and dimensions of each of its associated sections.

The hydrocyclone has an involute feed (see Figure 5) which begins as a circular opening, but becomes a slit entry into the upper swirl chamber. The swirl chamber consists of two cylindrical sections which are connected to each other and to a metal plate which is used to support the hydrocyclone on the scaffolding.

A noticeable discontinuity occurs at the junction of the swirl chamber and the conical section. The major conical diameter is approximately 3 mm larger than the diameter of the cylindrical section. This discontinuity was designed into the hydrocyclone to accommodate interchangeable components. The tolerances on the

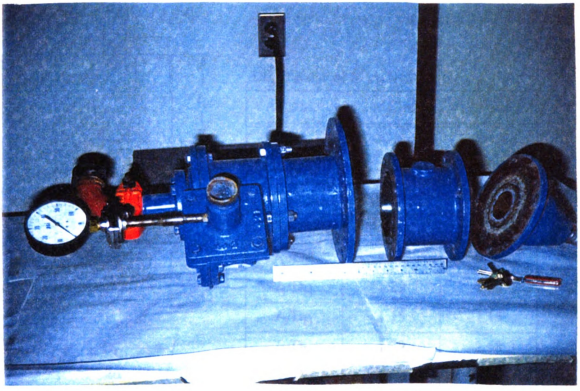

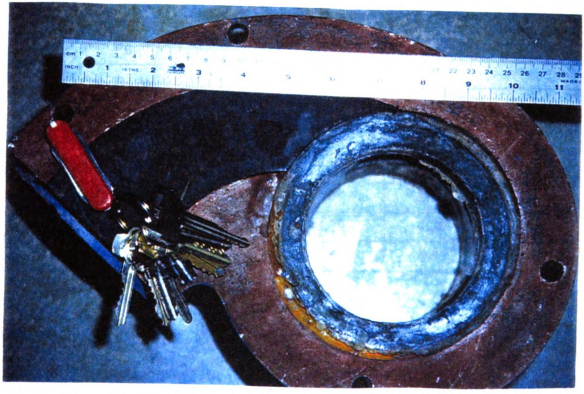

Figure 5: Photographs of the Krebs DB4-14 Hydrocyclone

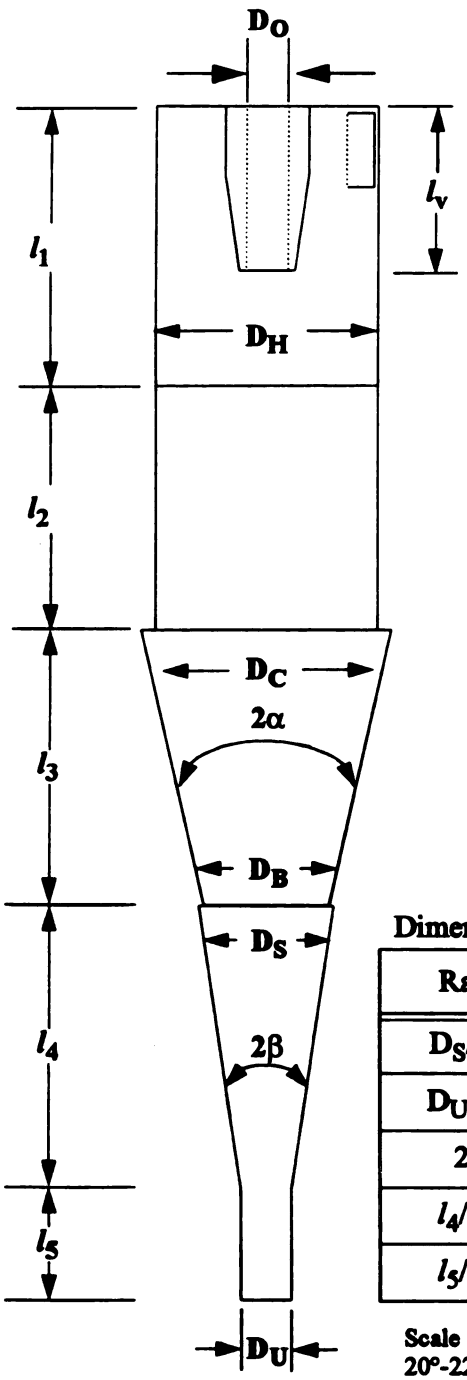

Dimensions of Main Section

Ratio	20° Cone	10° Cone
D_H	100 mm	100 mm
D_C/D_H	1.03	1.08
D_O/D_H	0.19	0.19
D_B/D_H	0.52	0.55
l_V/D_H	0.74	0.74
l_1/D_H	1.29	1.29
l_2/D_H	1.15	1.15
l_3/D_H	1.29	2.58
A_F/A_H	0.04	0.04
V_H/D_H^3	2.65	2.99
L_H/D_H	5.57	6.86

Dimensions of Underflow Fittings

Ratio	D_U = 10 mm	16 mm	22 mm
D_S/D_H	0.55	0.55	0.55
D_U/D_H	0.10	0.16	0.23
2β	20°	17.3°	14.3°
l_4/D_H	1.29	1.29	1.29
l_5/D_H	0.55	0.55	0.55

Scale 1:3.3
20°-22 Hydrocyclone Drawn

Figure 6: Dimensions of the Krebs Hydrocyclone and Fittings

polyurethane inserts are not as stringent as the machined parts, and the discontinuity avoids a reverse shelf which would adversely affect the flow patterns within the hydrocyclone.

The apex diameter of the hydrocyclone was controlled by using one of three interchangeable polyurethane socks. This allowed for three different underflow withdrawal schemes (see Figure 7). The withdrawal schemes are classified as conical, hyperbolic, and parabolic. These are defined according to the relative sizes of the major cone angle, 2α, and the angle of the underflow fitting, 2β. If 2α is less than 2β, then the underflow is parabolic. A hyperbolic scheme is produced when 2α is greater than 2β, and a conical withdrawal is formed when the two angles are equal.

The different combinations of α and β give six different withdrawal geometries. To distinguish between the different configurations, each geometry will be denoted by its major cone angle (i.e. 2α) followed by the size of the underflow diameter. For instance, the 20° cone in conjunction with the 16 mm underflow fitting gives a hyperbolic design and will be designated as the 20°-16 hydrocyclone. This style of designation was chosen because it allows for quick and easy recognition between the different configurations.

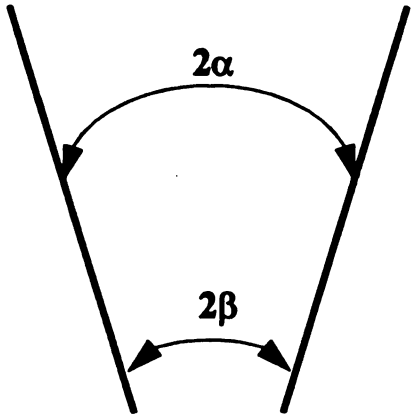

Conical Withdrawal

$2\alpha = 2\beta$

Cone	2α	2β
20°-10	20°	20°

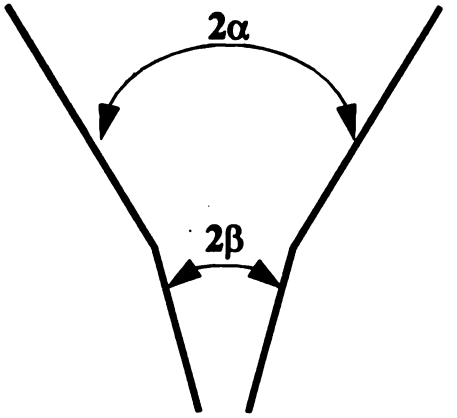

Hyperbolic Withdrawal

$2\alpha > 2\beta$

Cone	2α	2β
20°-16	20°	17°
20°-22	20°	14°

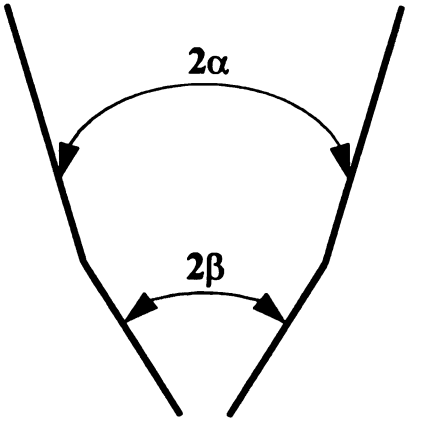

Parabolic Withdrawal

$2\alpha < 2\beta$

Cone	2α	2β
10°-22	10°	14°

Figure 7: Underflow Withdrawal Schees

2.4 Flow Circuit and Sampling Protocol

Light Medium Flow Circuit

The light medium flow circuit is shown in Figure 8. A 200 liter rigid HDPE tank, 100 mm hydrocyclone, and a centrifugal pump (Myers QP 30-3; 3 hp, 3450 rpm) are the major components of the light medium circuit. A two inch copper tube exits the bottom of the tank and feeds into the centrifugal pump. The copper tubing then extends from the pump and connects to a section of high pressure flexible hose. This hose is then attached to the feed inlet of the hydrocyclone.

A recycle flow stream through a 3/4 inch line provided additional agitation in the tank. A wide range of pressures could be tested by applying back pressure on the pump with the ball valve in the recycle line. Another ball valve located after the bypass was used to set the inlet pressure and flow rate to the hydrocyclone. The inlet pressure was measured with a 0-60 psi pressure gauge.

Valves located on the low pressure side of the pump allowed for the system to be drained. The placement of the valves was such that either the entire system including the tank or just the pumps could be drained.

Because of the abrasive nature of the microbubbles it was essential that the pumps be flushed at least every other day. A gate valve located just above the bypass

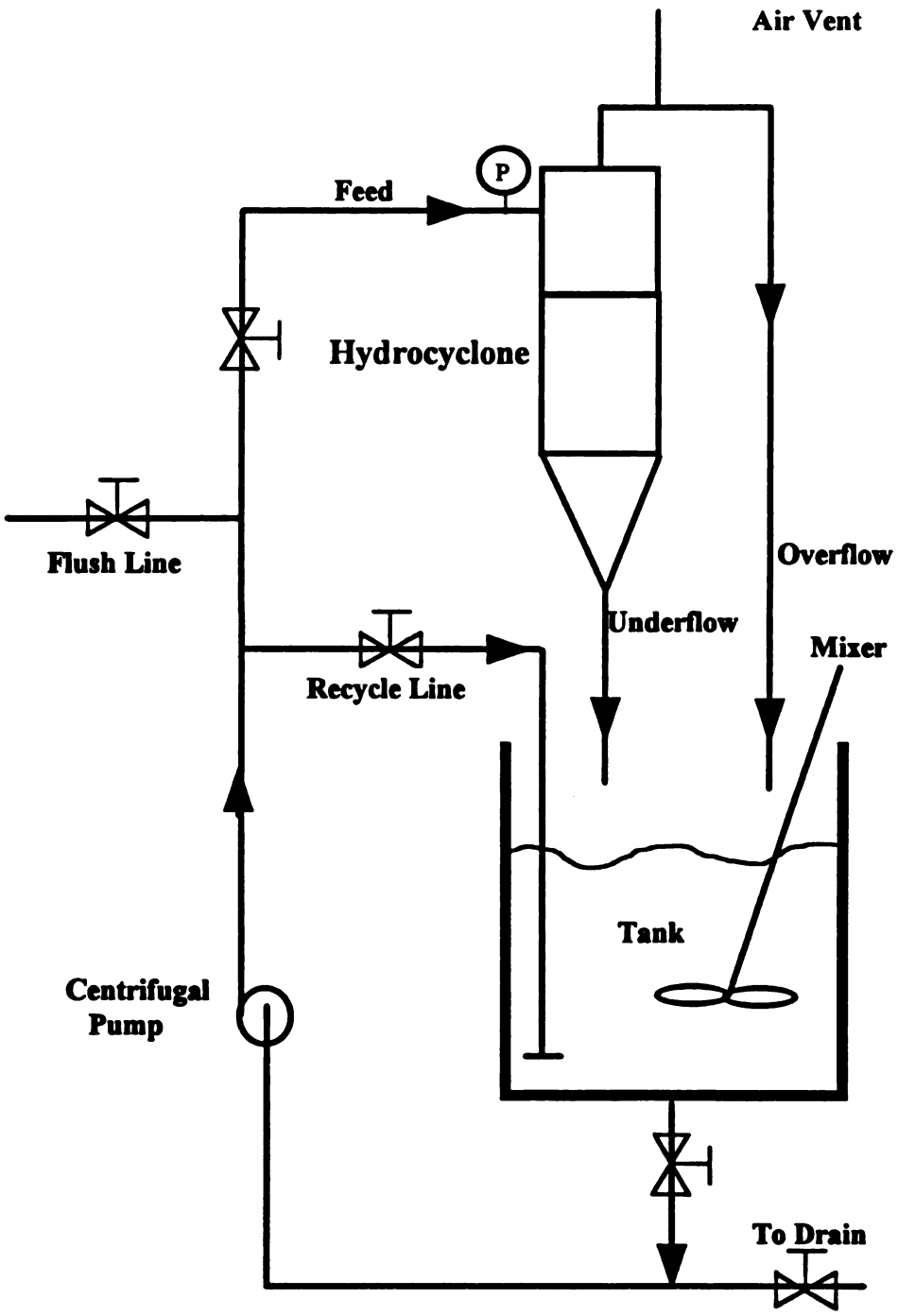

Figure 8: Schematic of Light Medium Flow Circuit

allowed clean water to be brought into the flow circuit. When the valves on the bypass, hydrocyclone feed, and tank outlet were closed, the valve on the flush line and the drain valve were opened. Water was then allowed to flow through the open pipes to remove any particles which were wedged in the pumps. Backpressure was periodically applied to ensure that the entire pump cavity was rinsed.

Density Measurements of the Light Medium

The density of the feed stream was an important parameter in this study. This was controlled by the amount of microbubbles added to the system. A gravimetric method was employed to determine the density of the system. This section describes the method to sample the feed and underflow densities.

To ensure proper mixing, the centrifugal pump was started and the suspension was allowed to recycle through the system for a minimum of five minutes at a flow rate of 40 *l*pm or greater. The overflow and underflow streams were then combined and allowed to collect in a three gallon container. The collected material was mixed to ensure homogeneity, and then a portion of the material in the container was poured into a graduated cylinder of known weight. The volume and weight of the suspension were measured, and then the density was calculated. This procedure was repeated five times and depending upon the average, the system

density was adjusted to the desired value by adding or removing microbubbles. This same procedure was used to determine the density of the underflow stream. Special care was taken to determine the volume of the suspension in the graduated cylinder before the microbubbles began to come out of suspension and form a froth at the liquid/air interface. When the microbubbles come out of suspension, the volume increases due to the packing of the microbubbles. If the volume of the suspension was measured after this occurred, then the calculated density would be less than its true value.

Sampling of HDPE and PP

Once the density of the glass microbubble/water suspension was known, the volume of the material in the tank was determined. This allowed for an estimate of the total mass flowing throughout the system. The material entrained in the piping and pump was considered insignificant and not taken into account when determining the total mass in the flow loop and the amount of thermoplastics to add to the system.

The suspension concentration of HDPE used in this study was approximately 0.1 wt.%. The separation of PP was also studied at feed concentrations of 0.1 wt.%. This low concentration was necessary because the centrifugal pumps would overheat when too many plastics were added to the system. The maximum amount

of thermoplastics used in this study was 0.5 wt.%. At this loading, the pump began to overheat and began to make uncharacteristic whirring noises. Future testing will employ progressive cavity pumps designed for multiphase flows.

Since some of the PP and HDPE were uncolored, each plastic was tested separately. Once either thermoplastic had been added to the tank, the pump was started. The valve between the bypass line and the feed line was adjusted to obtain the desired flow rate (see Figure 8). The system was allowed to run for a couple of minutes, and then the samples were collected. Samples were collected using a Number 20 standard sieve (850 μm). Two or three samples were collected for each inlet density. The samples were allowed to dry overnight and then weighed. After completing the separation runs for HDPE, the plastic was removed from the system using the sieves and replaced with PP. The separation experiments were repeated for PP using the same inlet pressures and hydrocyclone configuration as with HDPE.

2.5 Definition of Separation Performance

The following overall and component steady-state material balances for immiscible mixtures are used to evaluate the separation performance of the light medium hydrocyclone:

$$Q_F = Q_O + Q_U \qquad (2)$$

$$y_{iF}Q_F = y_{iO}Q_O + y_{iU}Q_O \ , \ i = 1, 2, 3, 4 \qquad (3)$$

where

Q_F = total volumetric flow rate of the feed stream

Q_O = total volumetric flow rate of the overflow stream

Q_U = total volumetric flow rate of the underflow stream

y_{iX} = volume fraction of constituent i (i = 1, 2, 3, 4) in stream X (X=F,O,U)

Each component of the process stream is identified by the index i (i= 1, HDPE; i = 2, PP; i = 3, glass microbubbles; and, i = 4, water). The mass density of each stream can be calculated in terms of the pure constituent densities, ρ°_i and the volume fractions, y_{iX}:

$$\rho_X = \sum_{i=1}^{4} y_{iX}\rho_i^\circ \ , \ X = F, O, U. \qquad (4)$$

The mass fraction of constituent i in stream X is $W_{iX} = \rho^\circ_i y_{iX} / \rho_X$.

An important, and useful, performance measure is the *stream purity coefficient* M_{1X} for HDPE:

$$M_{1X} \equiv \frac{y_{1X}\rho_1^\circ}{y_{1X}\rho_1^\circ + y_{2X}\rho_2^\circ} \ , \ X = F, O, U. \qquad (5)$$

A similar coefficient can be defined for PP:

$$M_{2X} = 1 - M_{1X} . \qquad (6)$$

The goal of the LMH separation process is to produce a high purity HDPE stream from a feed stream contaminated with PP. Current commercial recycling technology can produce a relatively clean HDPE/PP mixed stream for which $M_{2F}/M_{1F} = 0.01$. Unfortunately, this level of contamination causes the melt extruded product to have a grayish tint. If the light medium hydrocyclone could yield an underflow stream with $M_{2U}/M_{1U} = 0.001$, then this product may be an acceptable alternative to virgin HDPE.

The *recovery coefficients* for HDPE and for PP provide additional performance measures:

$$E_1 \equiv \frac{y_{1U} Q_U}{y_{1F} Q_F} \quad , \quad E_2 \equiv \frac{y_{2O} Q_O}{y_{2F} Q_F} \qquad \textbf{(7 a,b)}$$

E_1 and E_2 are also referred to as the yield of HDPE and PP, respectively. The ability of the separator to remove HDPE from the overflow stream and PP from the underflow stream can be evaluated in terms of the *overflow and underflow purity coefficients defined by*

$$\varepsilon_1 \equiv \frac{y_{1F} - y_{1O}}{y_{1F}} \quad , \quad \varepsilon_2 \equiv \frac{y_{2F} - y_{2U}}{y_{2F}} \qquad \textbf{(8 a,b)}$$

The overall and component material balances can be used to relate the above measures to the split ratio $S \equiv Q_U/Q_O$:

$$E_1 = \frac{\varepsilon_1 + S}{1+S} \tag{9}$$

$$E_2 = \frac{1+S\varepsilon_2}{1+S} \tag{10}$$

Note that if $\varepsilon_1 = 0$ (i.e., $y_{1O} = y_{1F}$) and $S > 0$, the recovery or yield of HDPE in the underflow stream is larger than zero ($E_1 = S / (1 + S)$). Under these conditions the hydrocyclone acts as a flow splitter. For positive values of ε_1, Eq. (9) implies that

$$\frac{S}{1+S} \le E_1 \le 1 \qquad \text{for } 0 \le \varepsilon_1 \le 1. \tag{11}$$

Similar observations can be made regarding the separation of PP, viz.,

$$\frac{1}{1+S} \le E_2 \le 1 \qquad \text{for } 0 \le \varepsilon_2 \le 1. \tag{12}$$

The utility of ε_1 and ε_2 as intrinsic separation performance measures stems from their insensitivity to the split ratio S.

If the LMH objective is to maximize the separation of HDPE and PP then a useful definition of separation efficiency is (see p. 166 in Bradley, 1952)

$$E \equiv \frac{y_{1U} Q_U + y_{2O} Q_O}{y_{1F} Q_F + y_{2F} Q_F}$$

$$E = Y_{1F} E_1 + (1 - Y_{1F}) E_2 \tag{13}$$

$$E = Y_{1F}\frac{\varepsilon_1 + S}{1+S} + (1 - Y_{1F})\frac{1+S\varepsilon_2}{1+S}$$

where

$$Y_{1F} \equiv \frac{y_{1F}}{y_{1F} + y_{2F}}. \tag{14}$$

Note that for $E_1=E_2$, the above definition for the separation efficiency reduces to $E=E_1=E_2$. For a given hydrocyclone design and for a specific HDPE/PP ratio in the feed stream, the separation efficiency E is determined by the Reynolds number ($Re_F \equiv 4Q_F / (\pi D_F \nu_C)$) and the density ratio Φ_F:

$$0 < \Phi_F \equiv \frac{\rho_F - \rho_3^\circ}{\rho_4^\circ - \rho_3^\circ} < 1 \tag{15}$$

where ρ°_4 and ρ°_3 represent, respectively, the densities of water and microbubbles. The split ratio S ($\equiv Q_U/Q_O$), which also affects E_1 and E_2, is determined by Re_F for a hydrocyclone operating with an air core.

The feed density ρ_F can be changed by the addition of microbubbles to the mixed plastic suspension (see Eq.(4)). As $\Phi_F \rightarrow 0$ (i.e., $\rho_F \rightarrow \rho^\circ_3$), both HDPE and PP will be separated to the underflow ($\varepsilon_1 \rightarrow 1$ and $\varepsilon_2 \rightarrow 0$). As $\Phi_F \rightarrow 1$ (i.e., $\rho_F \rightarrow \rho^\circ_4$), both HDPE and PP will be separated to the overflow ($\varepsilon_1 \rightarrow 0$ and $\varepsilon_2 \rightarrow 1$). For these limiting conditions, the separation efficiency becomes

$$E|_{\varepsilon_1=1,\varepsilon_2=0} = \frac{1+Y_{1F}S}{1+S} \tag{16}$$

$$E|_{\varepsilon_1=0,\varepsilon_2=1} = \frac{(1-Y_{1F})+S}{1+S} \tag{17}$$

Figure 9 illustrates the anticipated behavior of E as Φ_F changes. The density ratio Φ_1 (= 0.923) on Figure 9 corresponds to a feed stream having a density equal to HDPE (i.e., $\rho_F = \rho^\circ_1$). Likewise, Φ_2 (= 0.839) corresponds to $\rho_F = \rho^\circ_2$. The hypothetical example shown indicates that the maximum efficiency (E ≅ 0.9) occurs for $\Phi_{max} < \Phi_2 < \Phi_1$. The value of Φ_F for which $E_1 = 0.5$ is defined as $\Phi^{(1)}_{50}$. $\Phi^{(2)}_{50}$ is defined as the density ratio for which E_2 ($\Phi^{(2)}_{50}$) = 0.5. Figure 9 also illustrates the limiting values of E for $\varepsilon_2 = 0$ (Eq. (16)) and for $\varepsilon_1 = 0$ (Eq. (17)).

Eq. (13) shows that E depends on Y_{1F}, S, ε_1, and ε_2. The overflow and underflow purity coefficients, ε_1 and ε_2, are strongly influenced by Φ_F and Re_F. For low plastic loadings (y_{1F} and y_{2F} less than 0.05), ε_1 and ε_2 are expected to be independent of Y_{1F}. The split ratio, S, for a specific hydrocyclone operating with an air core is often a weak function of Re_F; therefore, the effect of Q_F on E is primarily through ε_1 and ε_2, not S. This observation partially motivates the use of a characteristic density related to the intrinsic performance of the hydrocyclone to scale the feed density. For instance, a cut-density characteristic of ε_1 could be

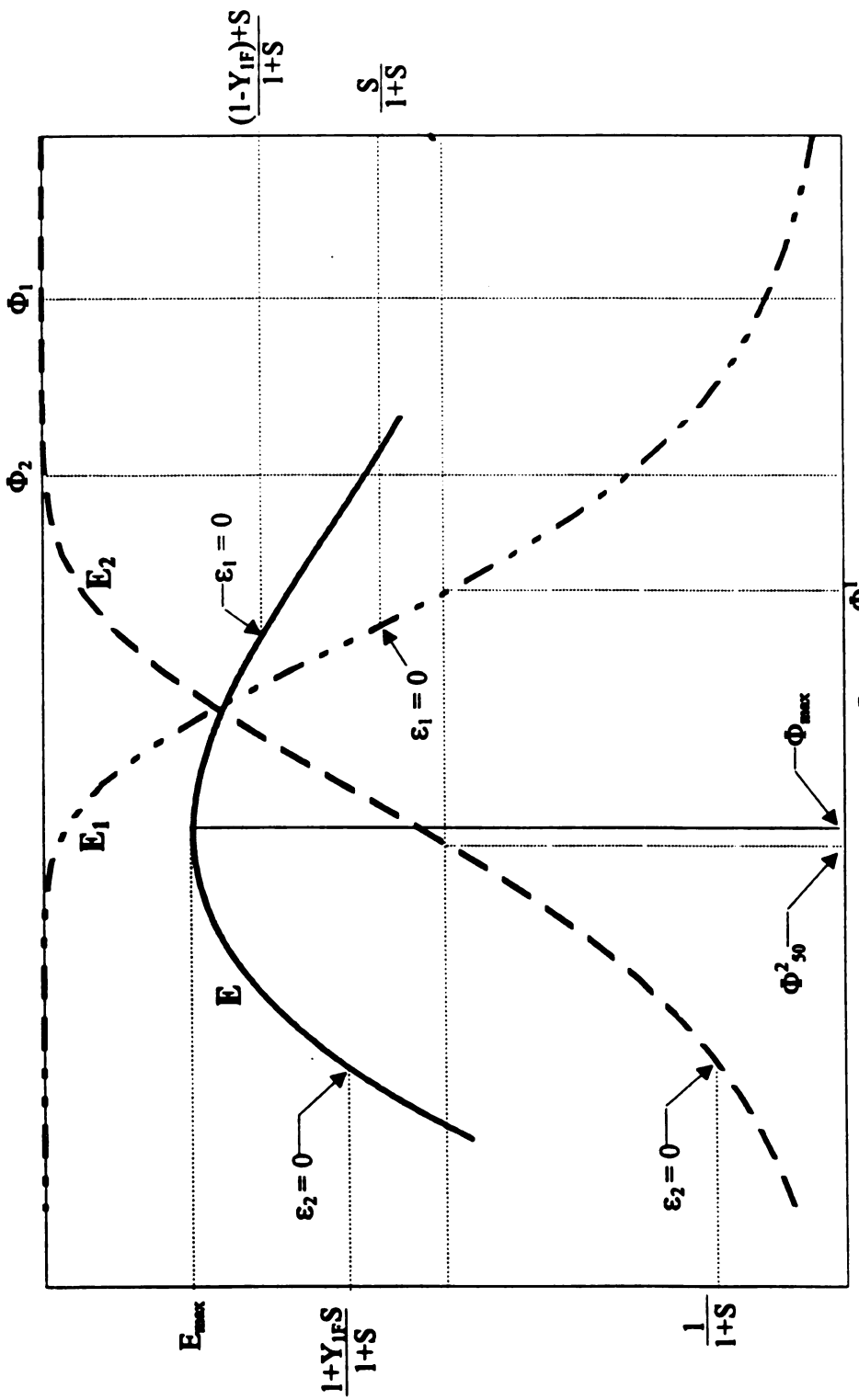

Figure 9: Separation Performance Measures for the Light Medium Hydrocyclone

defined as follows: $\varepsilon_1(\Phi^{(1)}_{50}) = 0.5$. For small split ratios, this cut-density would be comparable to the $\Phi^{(1)}_{50}$ associated with E_1 inasmuch as $E_1 \cong \varepsilon_1$ for $S << 1$. Using a cut-density related to ε_1, rather than to E_1, would provide an intrinsic measure of separation performance independent of the split ratio (Svarovsky, 1984). In this thesis, however, the cut-density associated with E_1 will be used to scale the feed density. Therefore, one of the objectives of this study is to test the following *similarity hypothesis*

$$E_1(\Phi_F, Re_F) \rightarrow E_1(\rho_F/\rho^{(1)}_{50}). \qquad (18)$$

The validity of Eq. (18) would clearly be an important simplification for engineering design and process development. In this study, experimental recovery data for HDPE were correlated with the dimensionless group ρ_F/ρ_{50} ($\rho_{50} \equiv \rho^{(1)}_{50}$ as defined previously) by using the following empirical equation:

$$E_1 = 1 - \exp\left[-\left(\frac{\rho_{50}}{\rho_F}\right)^b \ln(2)\right]. \qquad (19)$$

The parameters ρ_{50} and b were determined by using a least squares fit of the above equations to the data (E_1, ρ_F).

The stream purity coefficient M_{1U} (see Eq. (5)) is related to E_1 and E_2 by the following equation

$$M_{1U} = \frac{M_{1F}E_1}{M_{1F}E_1 + (1-M_{1F})(1-E_2)} \qquad (20)$$

where M_{1F} represents the stream purity coefficients for HDPE in the feed. For the special case of $M_{1F} = 0.5$, the above equation reduces to

$$M_{1U} = \frac{E_1}{E_1 + (1 - E_2)}. \qquad (21)$$

At some value of ρ_F/ρ_{50}, E_1 will be equal to E_2. It follows from Eq. (21) that at this point $M_{1U}=E_1=E_2$. Therefore, the experimental data presented hereinafter will be interpreted in terms of $E_1(\rho_F/\rho_{50})$ and $M_{1U}(\rho_F/\rho_{50})$ for a 50:50 mixture of HDPE and PP in the feed stream (i.e., $M_{1F}/M_{2F}=1$). The cross-over point (i.e., $E_1=M_{1U}$) gives the value of ρ_F/ρ_{50} for which $E=E_1=E_2=M_{1U}$.

2.6 Scope of Study

This study was designed to determine the feasibility of separating HDPE and PP using light medium technology, and to determine which design and operating parameters are important to the separation. The following factors were considered:

hydrocyclone design and operating conditions

- two cone configurations (20° and 10°)
- feed ratios between 48 lpm and 81 lpm
- split ratios between 0.1 and 2.0

light medium designs and feed densities

- two microbubble products (3M: K20 and K46)

- feed suspension densities from 1000 kg/m^3 down to 700 kg/m^3

HDPE and PP characteristics

- particle sieve size from 2-3 mm
- feed concentrations less than 0.5 wt.%
- separation and grinding experiments conducted separately

CHAPTER 3

EXPERIMENTAL RESULTS

3.1 Hydrodynamics

Hydrocyclone Flow Rates

The hydrocyclones were allowed to directly discharge to the atmosphere and, consequently, operated with an air core (see Figure 1). The air core is caused by the formation of a low pressure region in the center of the hydrocyclone created by the swirling motion of the fluid. The formation of the air core could have been avoided by placing backpressure on the overflow and underflow outlets with valves, but it was decided to allow for the free discharge of fluid back into the tank. This meant that the hydrocyclone was operated with low inlet pressures and pressure drops. Figures 10 and 11 show the flow rate/pressure drop curves for the 20° and 10° hydrocyclones. The curves show that the flow rates are related to each other by the equation: $|\Delta P| = KQ^n$. For the 20° cone, the values of K range from $8x10^{-5}$ to $1x10^{-4}$ bar/lpm^n, and n varies from 2.0 to 2.1. The K and n parameters for the 10° cone varied from $1x10^{-5}$ to $2x10^{-4}$ bar/lpm^n, and 1.8 to 2.5, respectively The values for n agree with typical values of 2 to 2.4 from the literature (see p. 91 Svarovsky, 1984).

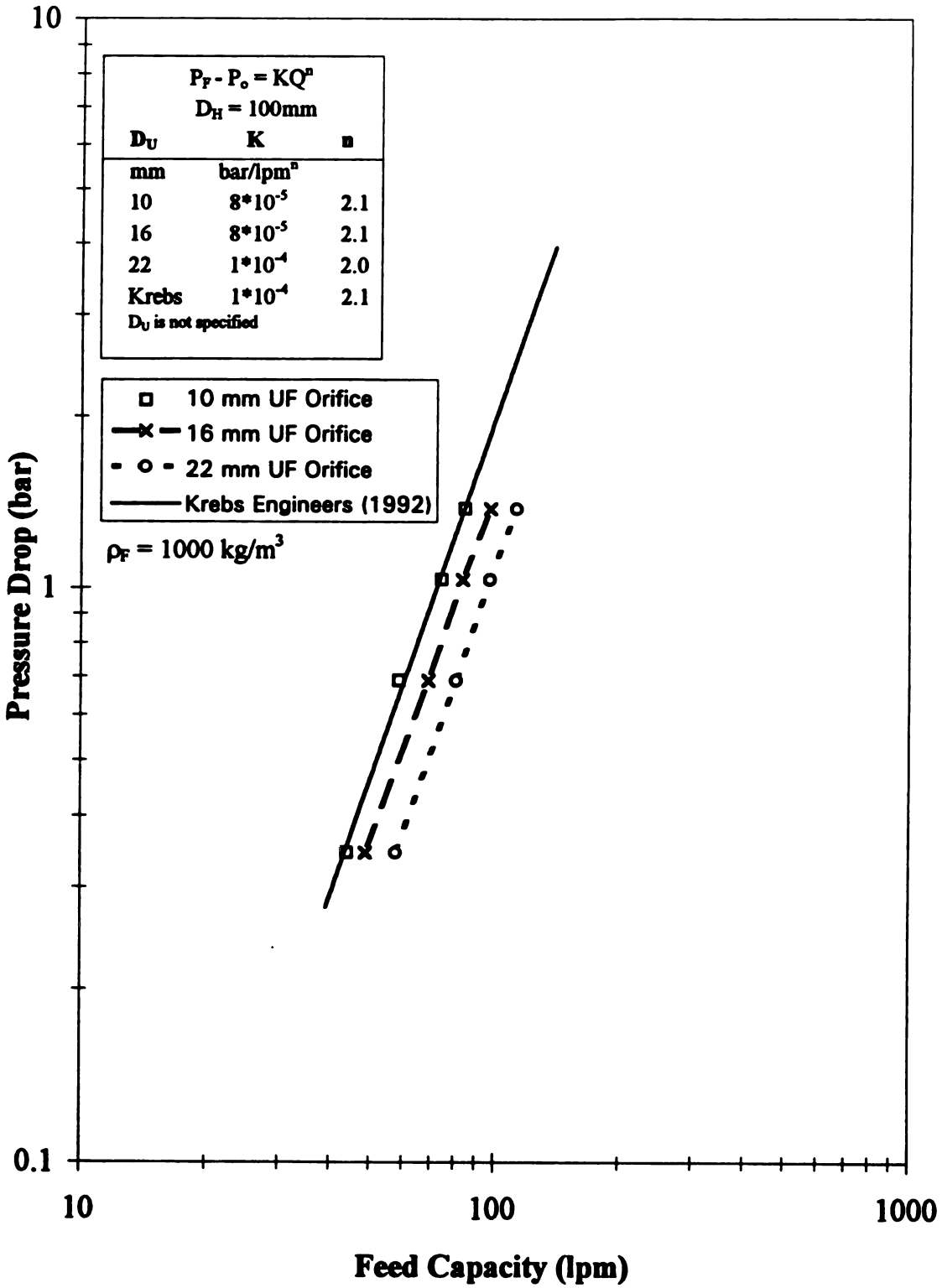

Figure 10: Pressure Drop vs Flow Rate for the 20° Hydrocyclone

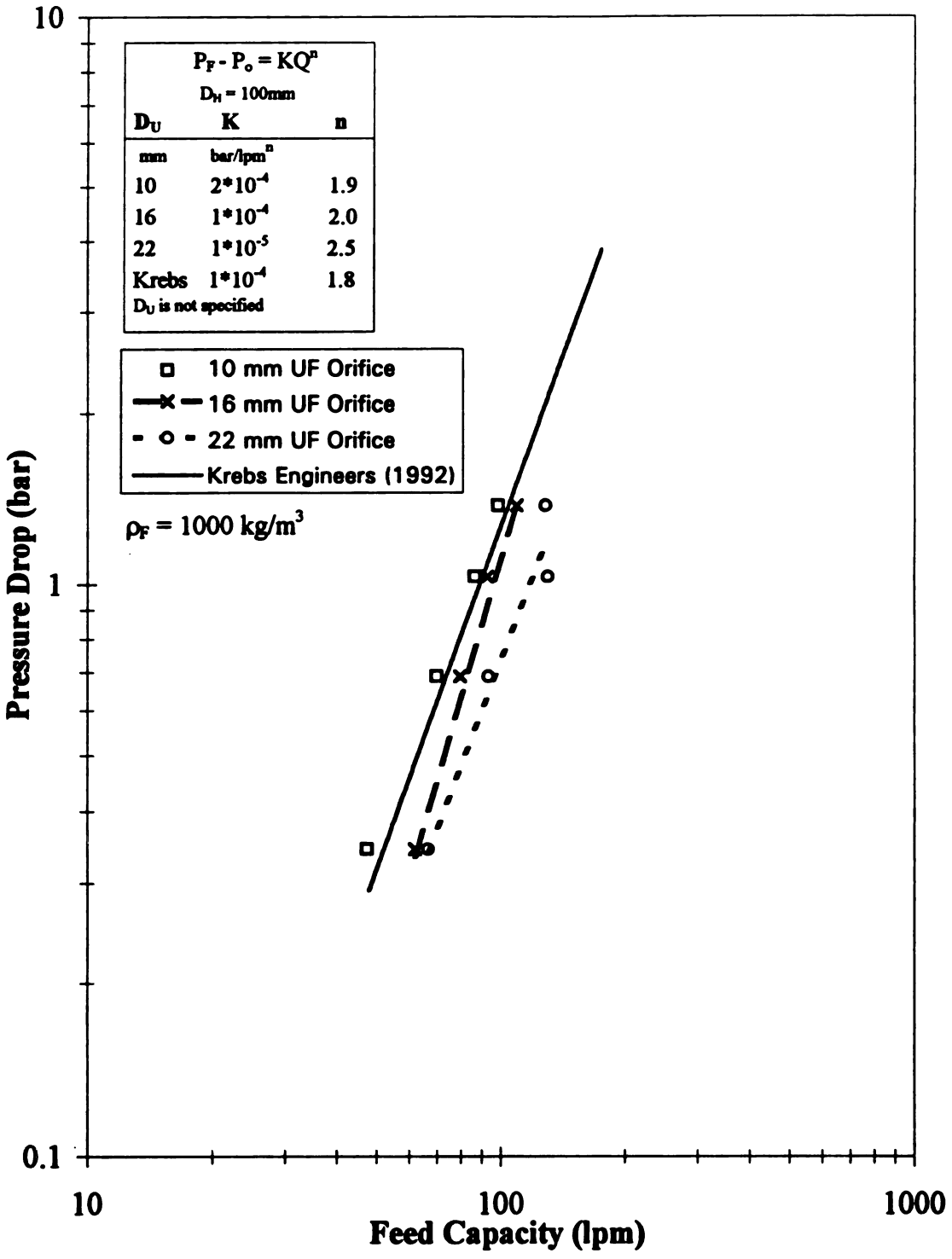

Figure 11: Pressure Drop vs Flow Rate for the 10° Hydrocyclone

Hydrocyclone Split Ratios

The split ratio for this study is defined by

$$S = \frac{Q_U}{Q_O} = \frac{\text{Volumetric Flow Rate UF}}{\text{Volumetric Flow Rate OF}} \qquad (22)$$

This operating parameter is greatly affected by the relative size of the underflow diameter to the overflow diameter, D_U/D_O. Figures 12 and 13 show how the split ratio changes as a function of underflow diameter and flow rate for the 20° and 10° hydrocyclones. The 22 mm underflow diameter has a much higher split ratio than either the 16 mm or the 10 mm underflow fittings. To a lesser extent, the flow rate also influences the split ratio. The higher flow rates have slightly lower split ratios.

3.2 Stability of Microbubble Suspension

Migration of Microbubbles

The migration of microbubbles has an important impact on the separation of PP and HDPE. Although microbubbles have the lowest density of any constituent in the LMH, their drift velocity is small because of their small size (see Section 2.1). Eq. (1) shows that the drift velocity increases as the acceleration $\langle u_\theta \rangle^2/r$ increases. Therefore, the migration of the microbubbles toward the core of the vortex increases as the pressure drop increases (i.e. as the flow rate increases). Figure 14 shows that microbubble migration makes the underflow suspension density larger than the feed density. Note that the underflow density initially rises quickly

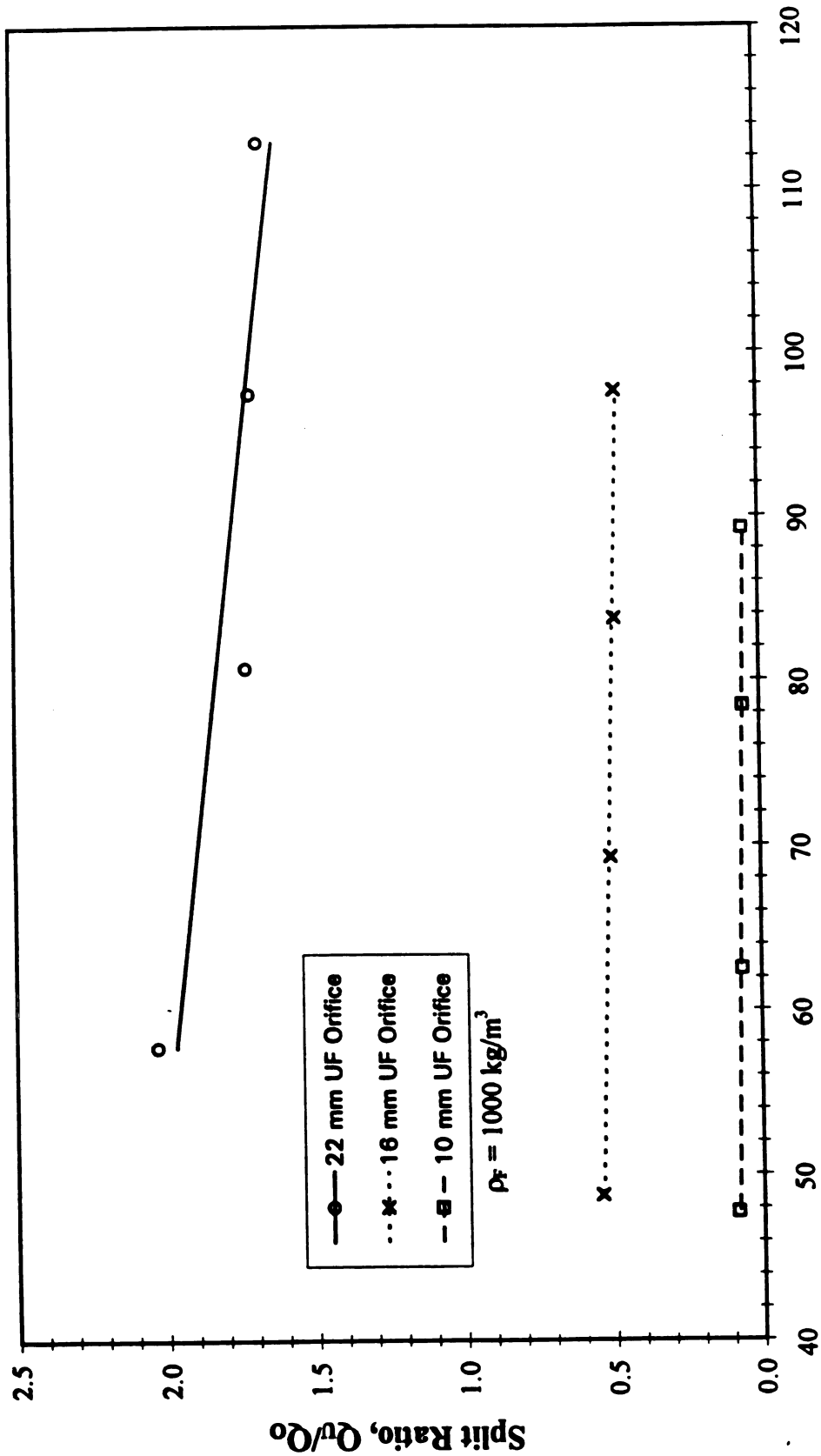

Figure 12: Split Ratio as a Function of Inlet Flow Rate for the 20° Hydrocyclone

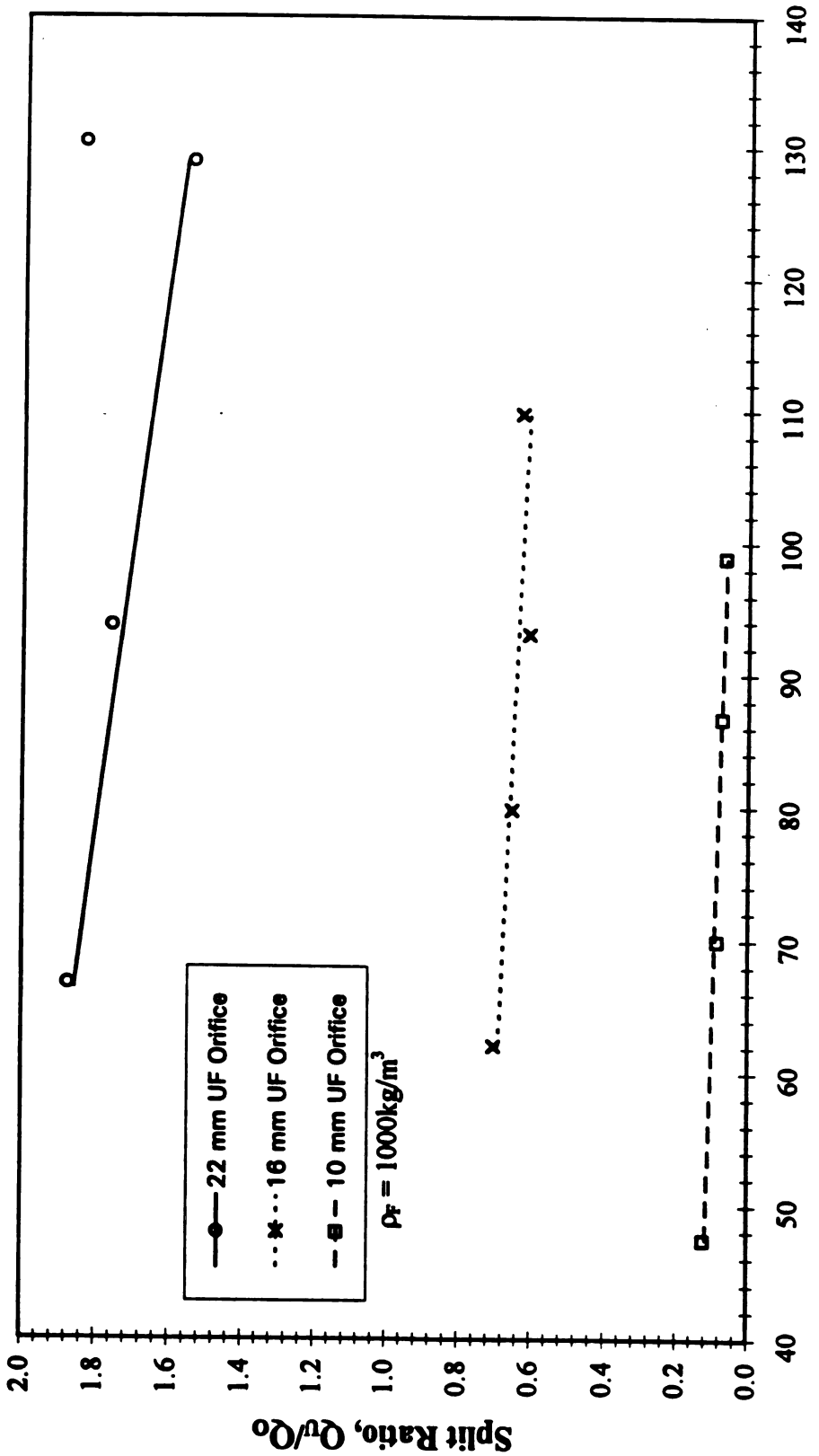

Figure 13: Split Ratio as a Function of Feed Flow Rate for the 10° Hydrocyclone

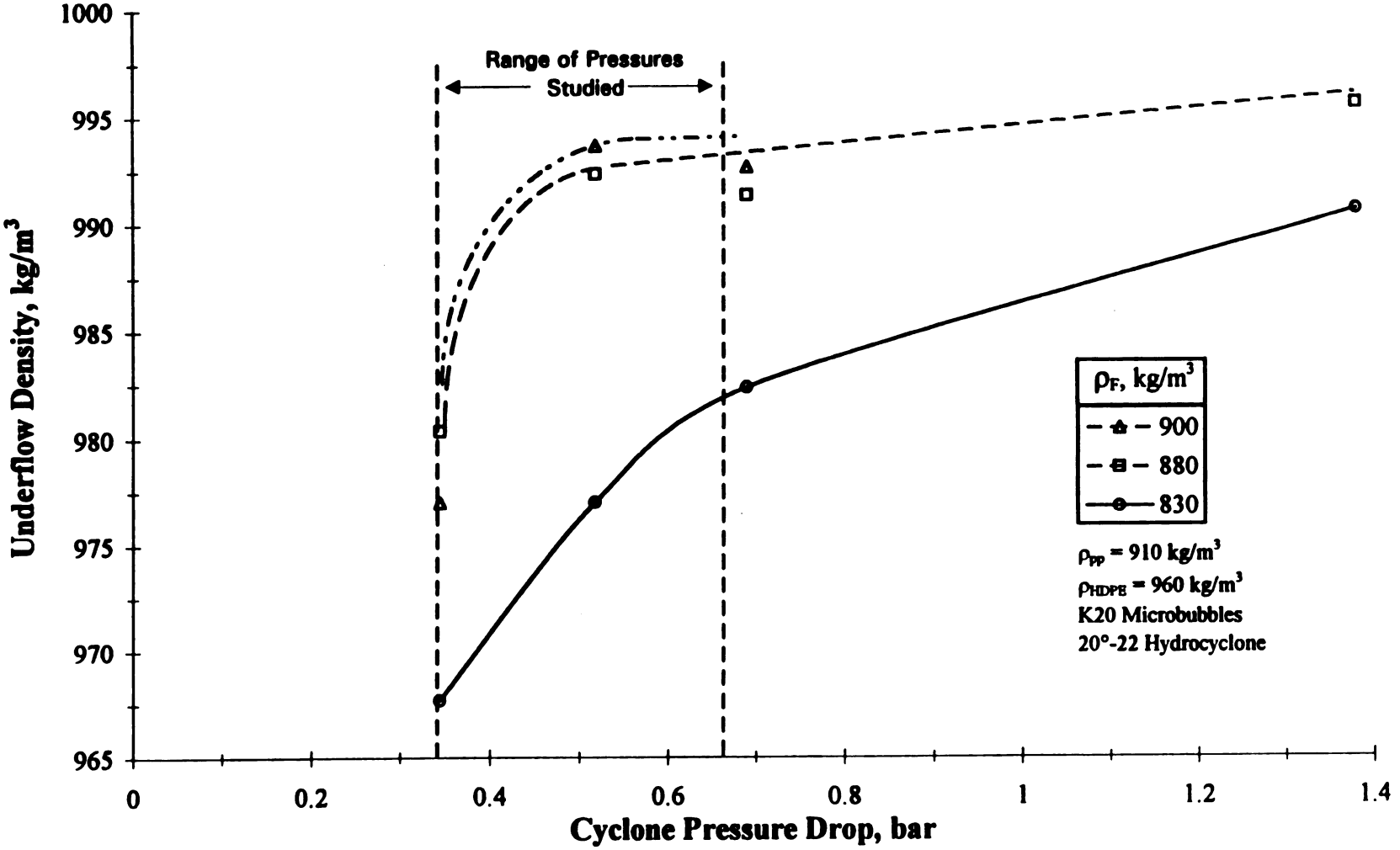

Figure 14: Underflow Density as a Function of Pressure Drop

with $|\Delta P|$ and then tapers off as the density of water is approached. For the conditions shown, the inlet velocity changes from 2.7 m/s for $|\Delta P| = 0.4$ bar, to 5.2 m/s for $|\Delta P| = 1.38$ bar. Also, for the feed conditions shown, it should be noted that the underflow density is much higher than either HDPE or PP even for feed suspension densities approaching 830 kg/m^3.

The hydrocyclone cannot be operated at pressure drops lower than 0.3 bar because of flow instabilities. However, because of adverse microbubble separation for $|\Delta P| > 0.7$ bar, the separation experiments were conducted for $0.3 < |\Delta P| < 0.7$ bar. The vertical dashed lines in Figure 14 show the range of operating pressures used in the experiments described later in this chapter. Clearly, the 20°-22 hydrocyclone does not favor the development of an underflow suspension density which would support the separation of HDPE and PP for feed densities larger than 830 kg/m^3.

Microbubble Break-Up

While conducting the performance studies, it was noted that the microbubbles were breaking and, consequently, changing the density of the underflow because broken glass would preferentially report to the underflow. The inability of the microbubbles to withstand the stresses within the flow circuit would clearly limit the practical utility of the LMH. To counter the break-up, the system was

periodically cleaned, but some broken material was always present due to the continuous recycle arrangement of the flow circuit. This section attempts to quantify the amount of microbubble breakage in the LMH.

The break-up of microbubbles was studied using a centrifugal pump and a low shear progressive cavity pump. The progressive cavity pump was used to continuously recycle the suspension through a flow loop consisting of a 17 ft section of 1" diameter pipe. The centrifugal pump was part of the light medium flow circuit (see Figure 8).

Figure 15 shows the break-up of the K20 microbubbles in the two flow circuits. Initially, there is approximately 6% microbubbles broken in a fresh batch. The manufacturer's number for the amount broken is 4%. The amount of microbubbles broken in the centrifugal pump circuit rises very quickly and then tapers off. About 40 wt.% of the microbubbles were broken after four hours of continuous operation. This is in contrast to the break-up in the low shear pump circuit which showed a steady increase in the amount of broken microbubbles. The amount broken, however, is well below the amount of breakage experienced in the centrifugal pump circuit. It is not know if the amount of broken material in the two systems will reach the same asymptotic value.

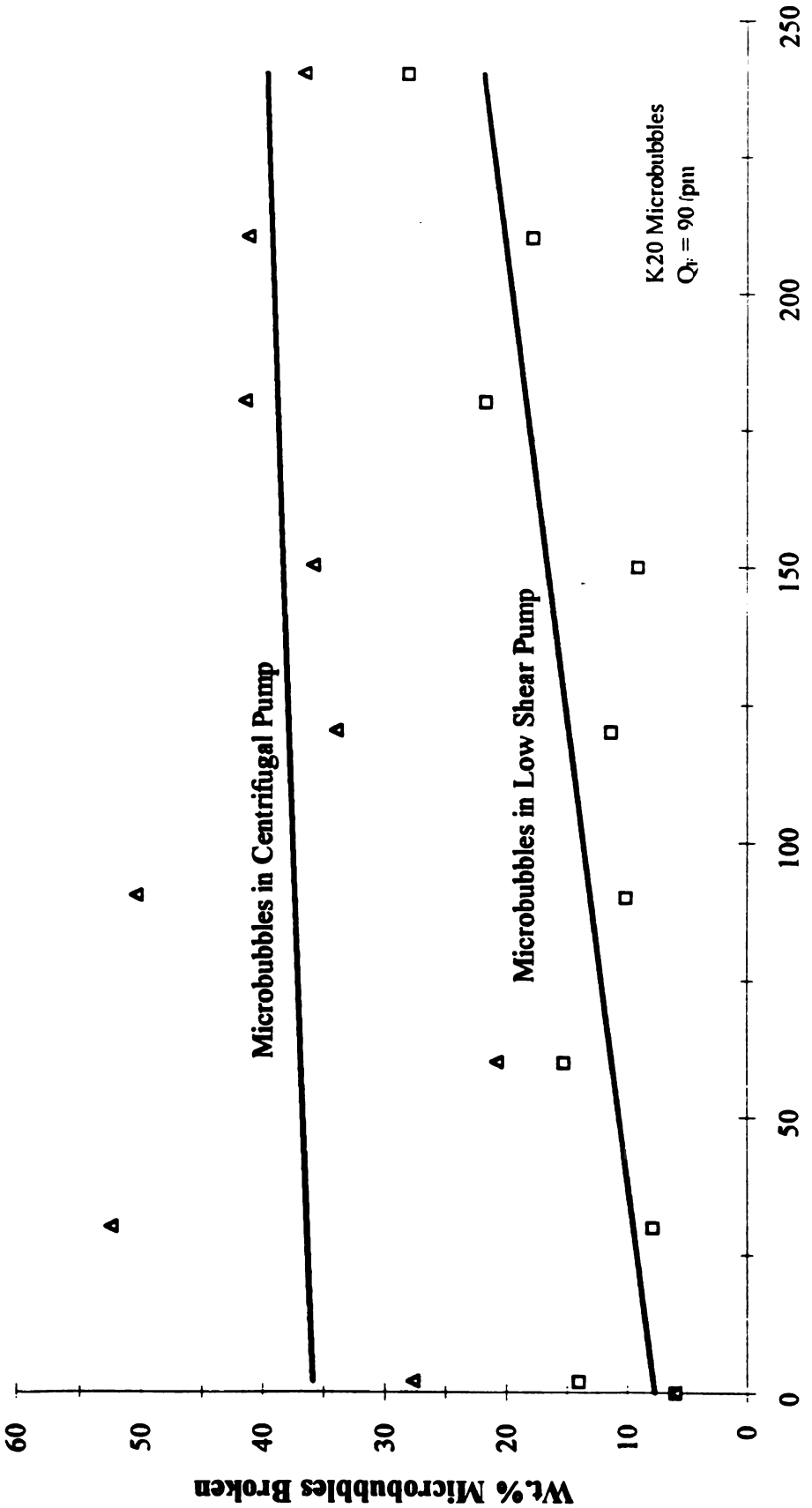

Figure 15: Comparison of Microbubble Break-Up in Centrifugal and Progressive Cavity Pumps

Figure 16 shows the break-up of microbubbles in the progressive cavity flow circuit for a longer period of time. On this chart, the y-axis is the volume percent of broken material instead of the weight percent of broken microbubbles as was used on the previous graph. This procedure was chosen because it provided a quick measure to determine any trends in the break-up process. The second experiment was performed to determine if the breakage would reach a plateau, and to ascertain the effect of restarting the flow system. As shown, the amount of microbubbles broken tapered off around four hours into the study. Once this plateau was achieved, the system was shut down and the microbubbles were allowed to settle out of suspension overnight. The loop was then restarted and samples collected. The amount of broken microbubbles began to increase again and did not approach a new plateau during this four hour study. Also, the figure shows that increasing the flow rate did not influence the amount of microbubbles broken in the system. This would have been noted by an increase in the rate of microbubble break-up.

3.3 Separation Performance

As stated in Chapter 1, the objective of this study was to determine the separation performance of the LMH. This section describes the effect of the design and operating variables on the performance of the light medium hydrocyclone. Figure 17 is a representative sample of the type of separation obtained.

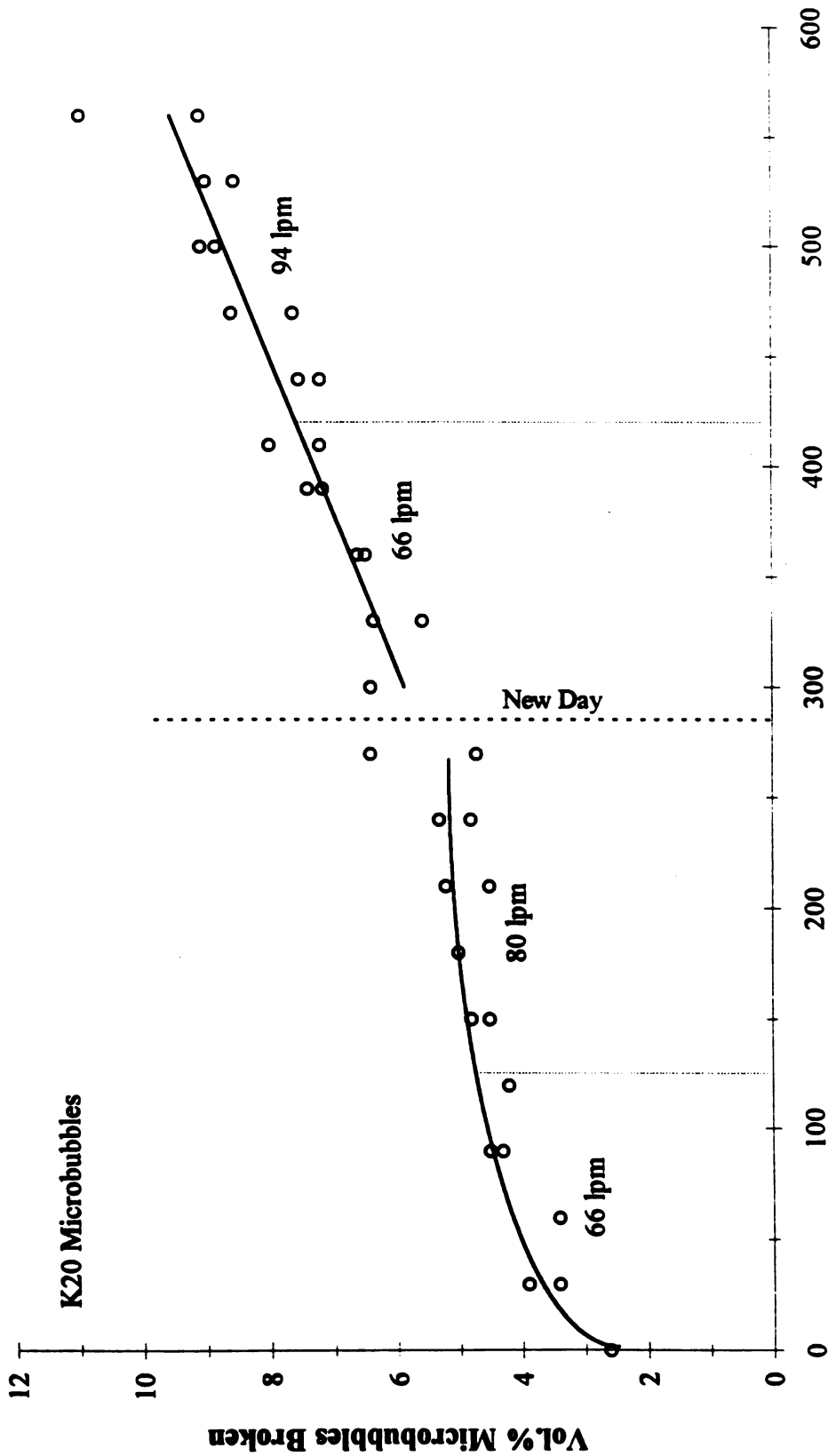

Figure 16: Microbubble Break-Up with Time in a Progressive Cavity Pump

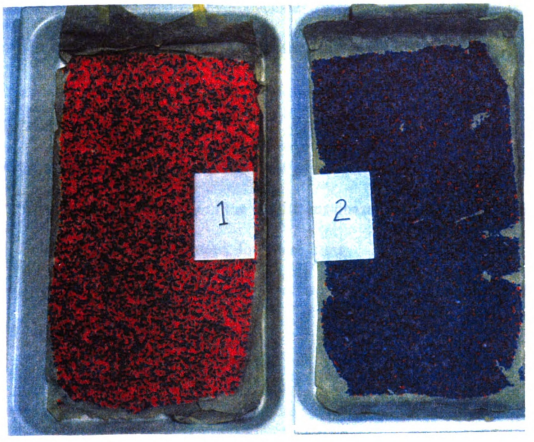

Operating Conditions
20°-22 Hydrocyclone
$|\Delta P| = 0.7$ bar
$Q_F = 81$ lpm
$\rho_F = 800$ kg/m^3

Figure 17: Photograph of Separation of PP and HDPE in a Light Medium Hydrcyclone

The initial feed composition was approximately 60% HDPE (blue) and 40% PP (orange). The figure shows that a relatively clean stream of HDPE (>90%) may be obtained using a light medium hydrocyclone. Note that the feed density is lower than 830 kg/m^3, as recommended by the results shown in Figure 14.

Effect of Split Ratio

For this study, the inlet pressure was fixed at 1.4 bar, and the K20 microbubbles were used to lower the density of the continuous phase. The 20°-22, 20°-16, and 20°-10 hydrocyclones were used for these runs. The split ratios for these configurations were 2.0, 0.6, and 0.1, respectively and the feed rates were 58, 49, and 48 lpm.

Figure 18 shows the effect of increasing the split ratio on E_l and M_{lU}. The data fall on the same similarity curves when correlated with the reduced density, ρ/ρ_{50}. The values of ρ_{50} were determined to be 830, 750, and 660 kg/m^3 for S equal to 2.0, 0.6, and 0.1, respectively. The long tails on the right side of the graph for the two curves are associated with the 20°-10 hydrocyclone configuration with a very low cut-density of 660 kg/m^3. Also note that at high yields the inlet densities are much lower than the densities of either HDPE or PP.

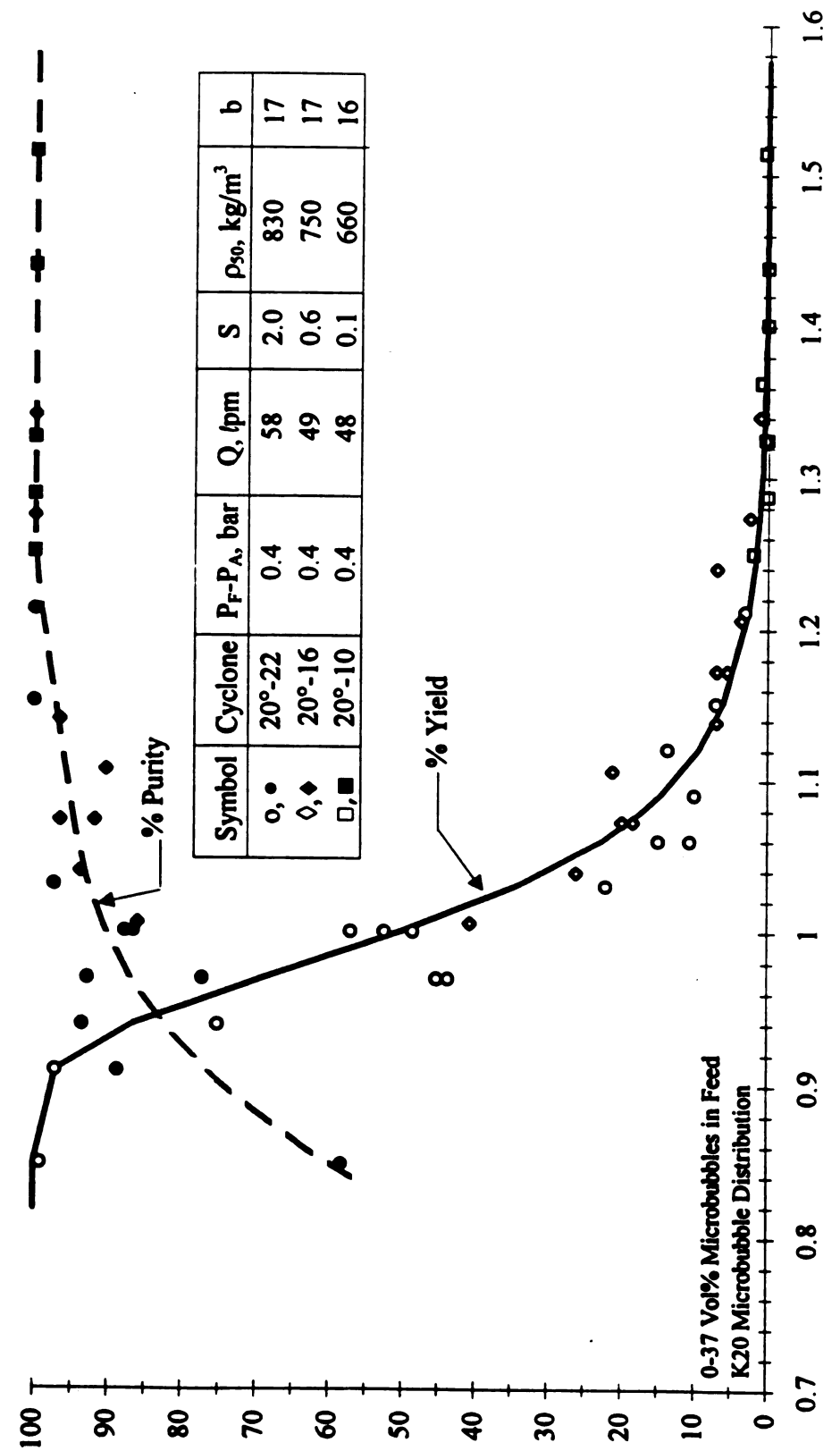

Symbol	Cyclone	P_F-P_A, bar	Q, lpm	S	ρ_{50}, kg/m^3	b
o, •	20°-22	0.4	58	2.0	830	17
◊, ◆	20°-16	0.4	49	0.6	750	17
□, ■	20°-10	0.4	48	0.1	660	16

Figure 18: The Effect of Split Ratio on the Performance of a Light Medium Hydrocyclone

Effect of Pressure Drop

The feed velocity is an important parameter in that the tangential component of the velocity, $\langle u_\theta \rangle$, is directly related to this variable. With an inlet of constant cross-sectional area, the feed velocity is directly proportional to flow rate. The 20°-22 hydrocyclone was operated at $|\Delta P|$ of 0.4 and 0.7 bar with a corresponding inlet velocity of 2.7 m/s to 3.7 m/s, respectively. As $|\Delta P|$ increases from 0.4 to 0.7 bar, the split ratio decreases from 2.0 to 1.7. The effect of this change in pressure drop on the recovery coefficient E_1 and the HDPE purity, M_{1U}, is shown in Figure 19. Both the yield and purity curves seem to correlate with ρ_F/ρ_{50}. The value of ρ_{50} for the higher inlet velocity, 780 kg/m^3, is well below the value of 830 kg/m^3 for the smaller inlet velocity.

Microbubble Distribution

As concluded from Figure 13, the segregation of microbubbles in the LMH is significant. The migration is caused by the large density difference between the K20 microbubbles and water ($\rho_C - \rho_B$ = 790 kg/m^3). To reduce this migration, a smaller, more dense distribution (K46) was used ($\rho_C - \rho_B$ = 560 kg/m^3). The K46 distribution has approximately 1/4 the Stokes' drift velocity of the K20 distribution for a given acceleration (see Eq.(1)). For this comparison, the 20°-22 hydrocyclone was operated at a pressure drop of 0.4 bar. These parameters were

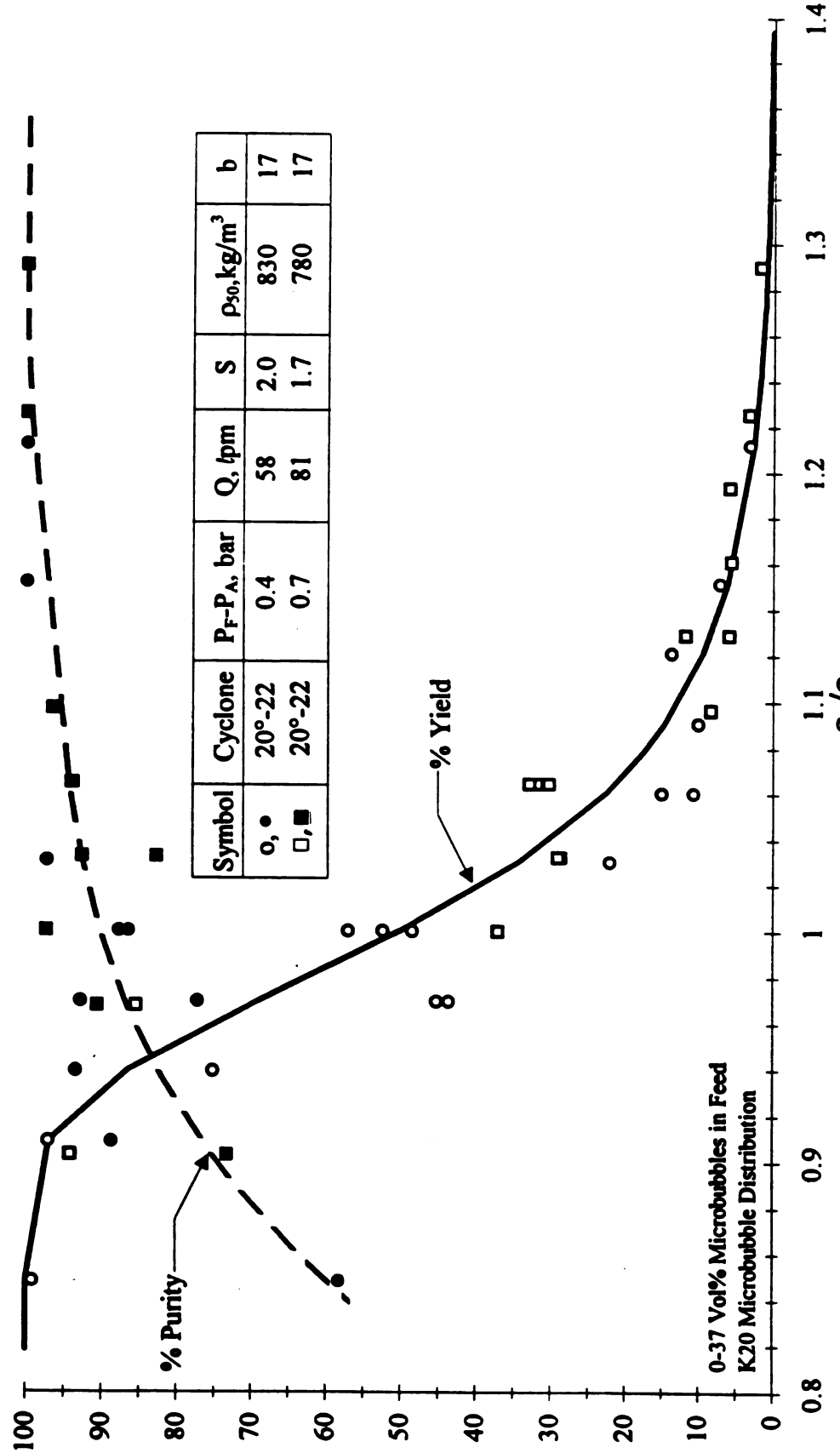

Figure 19: The Effect of Flow Rate on the Performance of a Light Medium Hydrocyclone

chosen because the combination of high split ratios and low inlet pressures (velocities) produced the highest yield for a given inlet density.

Figure 20 shows that the recovery of HDPE in the underflow stream (yield) as well as the % purity (M_{1U} x 100%) for two different microbubble distributions can be correlated with ρ_F/ρ_{50}. Again, the difference between the performance of the two distributions is ρ_{50}. The value of ρ_{50} for the K46 (smaller) distribution is 870 kg/m^3 compared to 830 kg/m^3 for the K20 (larger) distribution. As previously noted, the feed density of the suspension at high yields are well below the densities of HDPE and PP.

Cone Angle

Figure 21 shows the performance of the LMH with hydrocyclones of different angles. The 20°-22 and 10°-22 hydrocyclones were used for this comparison. The 10°-22 hydrocyclone was operated at a pressure drop of 0.4 bar while the 20°-22 hydrocyclone was run at 0.5 bar. The different operating pressures ensured that the two hydrocyclones had the same volumetric flow rate and, consequently, the same feed velocity and split ratio. The K46 microbubble distribution was used in these trials to vary the inlet density from the density of pure water ($\approx$ 1000 kg/m^3) down to 750 kg/m^3. The curves show approximately the same performance when plotted as a function of the reduced density ρ_F/ρ_{50}. The 10°-22 hydrocyclone has a

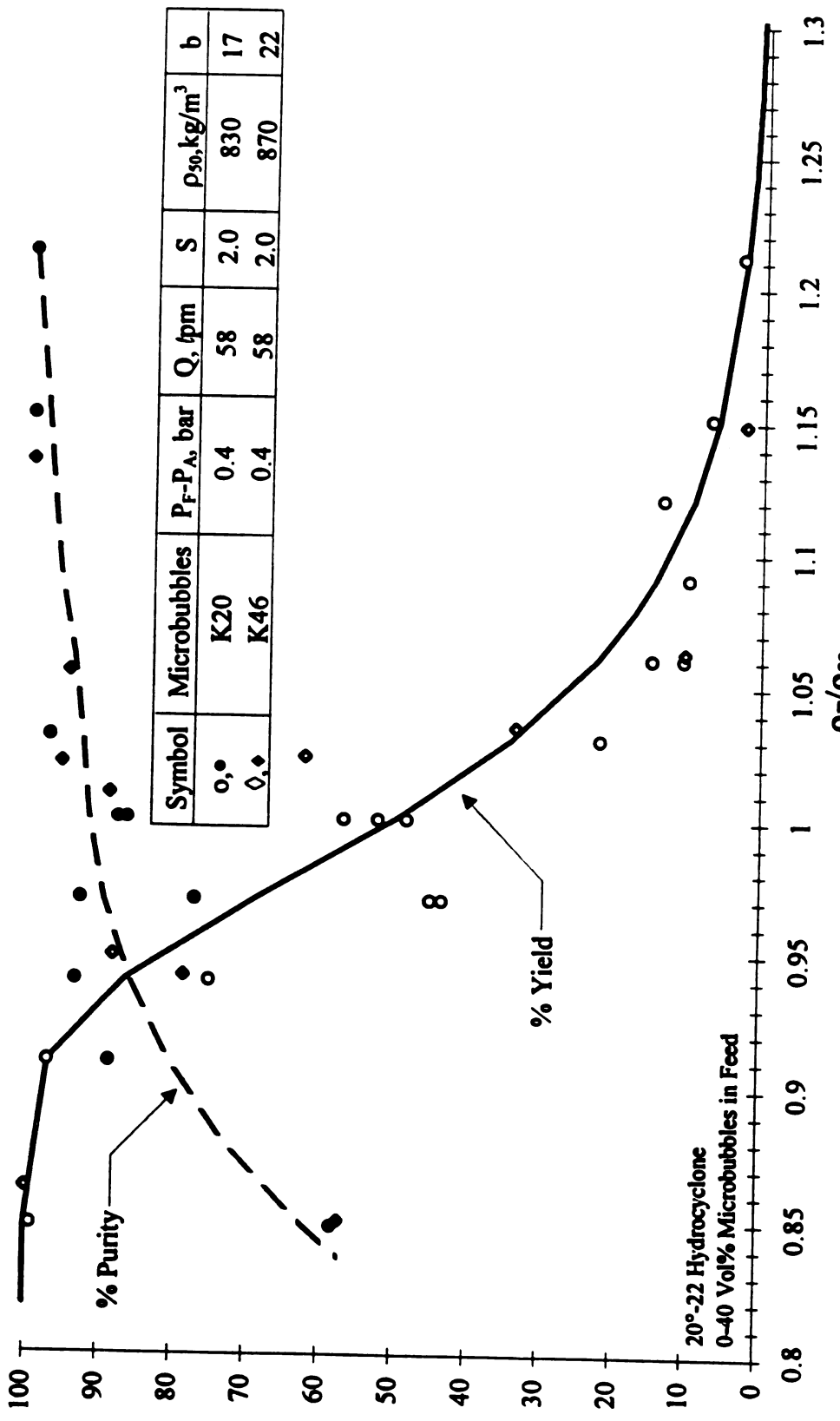

Symbol	Microbubbles	P_F-P_A, bar	Q, lpm	S	ρ_{50},kg/m^3	b
o,●	K20	0.4	58	2.0	830	17
◊,♦	K46	0.4	58	2.0	870	22

Figure 20: The Effect of Microbubble Size Distribution on the Performance of a Light Medium Hydrocyclone

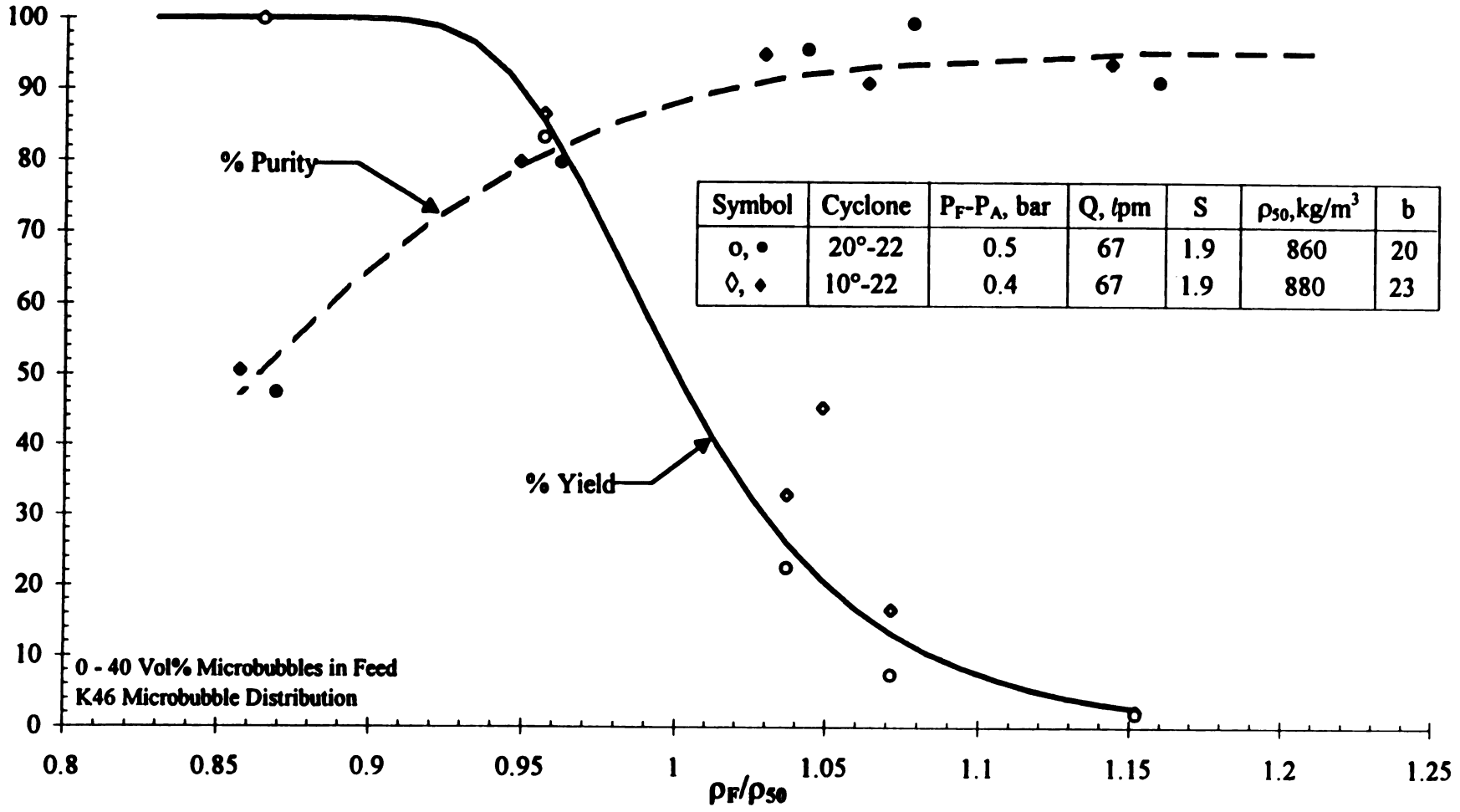

Figure 21: The Effect of Cone Angle on the Performance of a Light Medium Hydrocyclone

higher ρ_{50} (880 kg/m^3) than the 20°-22 hydrocyclone (860 kg/m^3). The difference for these two cone angles is smaller than the other comparisons.

Effect of HDPE Concentration

The concentration of HDPE in the feed (i.e., y_{1F}) may greatly affect the economic feasibility of the LMH. Experiments were conducted to determine the effect of y_{1F} on E_1 for the 20°-22 hydrocyclone using the K20 microbubbles with a feed density of 780 kg/m^3. Figure 22 shows that the yield (i.e., E_1) is independent of HDPE concentration over the range studied (100-5000 ppm). The data at a pressure drop of 0.4 bar (Q_F = 58 lpm) agree well with the same operating point shown on Figure 16. For HDPE feed concentrations above 1000 ppm, the feed pressure was increased to 0.5 bar (Q_F = 64 lpm) to avoid clogging. The experiment was terminated at an HDPE concentration of 5000 ppm because the centrifugal pump could no longer handle the solids loading.

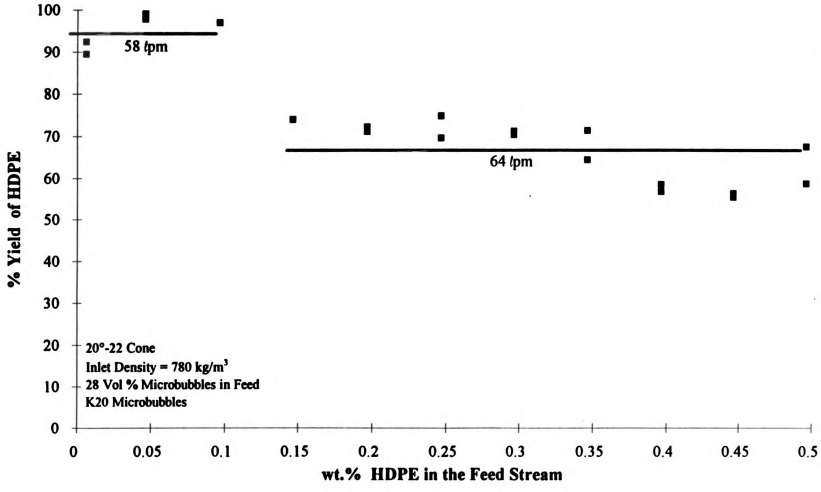

Figure 22: Percent Yield of HDPE in a Light Medium Hydrocyclone as a Function of HDPE Feed Concentration

CHAPTER 4

DISCUSSION OF RESULTS

4.1 Hydrodynamics

Pressure Drop/Flow Rates

A small incremental increase in the cost of processing HDPE could limit the practical utility of the LMH because of the low profit margins associated with the recycled material. Consequently, the economics of the process is very important. One variable which may be used to estimate operating costs is the pressure drop over the hydrocyclone. Energy consumption in the LMH can be estimated by calculating the power ($\mathcal{P} = Q \cdot |\Delta P|$) required to operate the hydrocyclone. For the hydrocyclone configurations and flow rates studied, the energy consumed per unit time (i.e. power) required to operate the LMH was estimated to be 300 W for Q_F = 100 lpm and $|\Delta P|$ = 1.4 bar. This corresponds to 0.3 kW·h for one hour of continuous operation. Thus, a lower bound on the operating cost to process 200 kg/h of HDPE is 2¢/h, based on an energy cost of 7.6¢/kW·h and 4 wt.% plastics loadings.

Split Ratio

Figures 12 and 13 show the strong dependence of the split ratio (Q_U/Q_O) on the underflow diameter. This strong dependence is actually a function of the ratio of the underflow diameter to that of the overflow which was fixed for the Krebs hydrocyclone. Svarovsky (see p.100) states that the split ratio is proportional to $(D_U/D_O)^{3.31}$. Using the data from Figures 12 and 13, the exponent on D_U/D_O was determined to be 3.75 for the 10° hydrocyclone and 3.26 for the 20° hydrocyclone.

It was also noted in Section 3.1 that the split ratio was a weak function of $|\Delta P|$. This dependence is given by Svarovsky as $S \propto |\Delta P|^{-0.24}$ (see p. 100). Values of this exponent were determined to be -0.20 and -0.32 for the 10° and 20° hydrocyclones, respectively. These values correlate well with the literature value of -0.24.

Pressure Loss Coefficient

Bradley states (see p. 90) that the major source of pressure loss in a hydrocyclone is from the centrifugal head, and that other sources of pressure loss are negligible. The pressure loss coefficient is defined as:

$$C_P = \frac{|\Delta P|}{\rho v^2 / 2}, \qquad (22)$$

where v represents the bulk average velocity of the feed and r is the density of water (no microbubbles).

Figures 23 and 24 show the pressure loss coefficient as a function of Reynolds number. It appears that C_P is independent of the Reynolds number, indicating that the viscous losses are small compared to the losses associated with the centrifugal head. The values for C_P range from 10 to 17 for the 20° hydrocyclone, and are between 7 and 15 for the 10° hydrocyclone.

Knowledge of the pressure loss coefficient allows an estimation of the values for α and N from the following equation (see p.90 Bradley, 1965):

$$C_P = \frac{\alpha^2}{N}\left[\left(\frac{D_H}{D_U}\right)^{2N} - 1\right] \qquad (23)$$

For $D_H/D_U = 4.5$, a value of $C_P = 19$ results when N and α are set equal to one. This should be an upper bound on the pressure loss coefficient. The curves on Figures 23 and 24 show this to be valid. Also, by solving Eq. (23) for α, and requiring that $\alpha \leq 1$ places an upper bound on the value of N. This corresponding value of N was determined to be approximately 0.75 for $C_p = 11$, $\alpha = 1$, and $D_H/D_U = 4.5$.

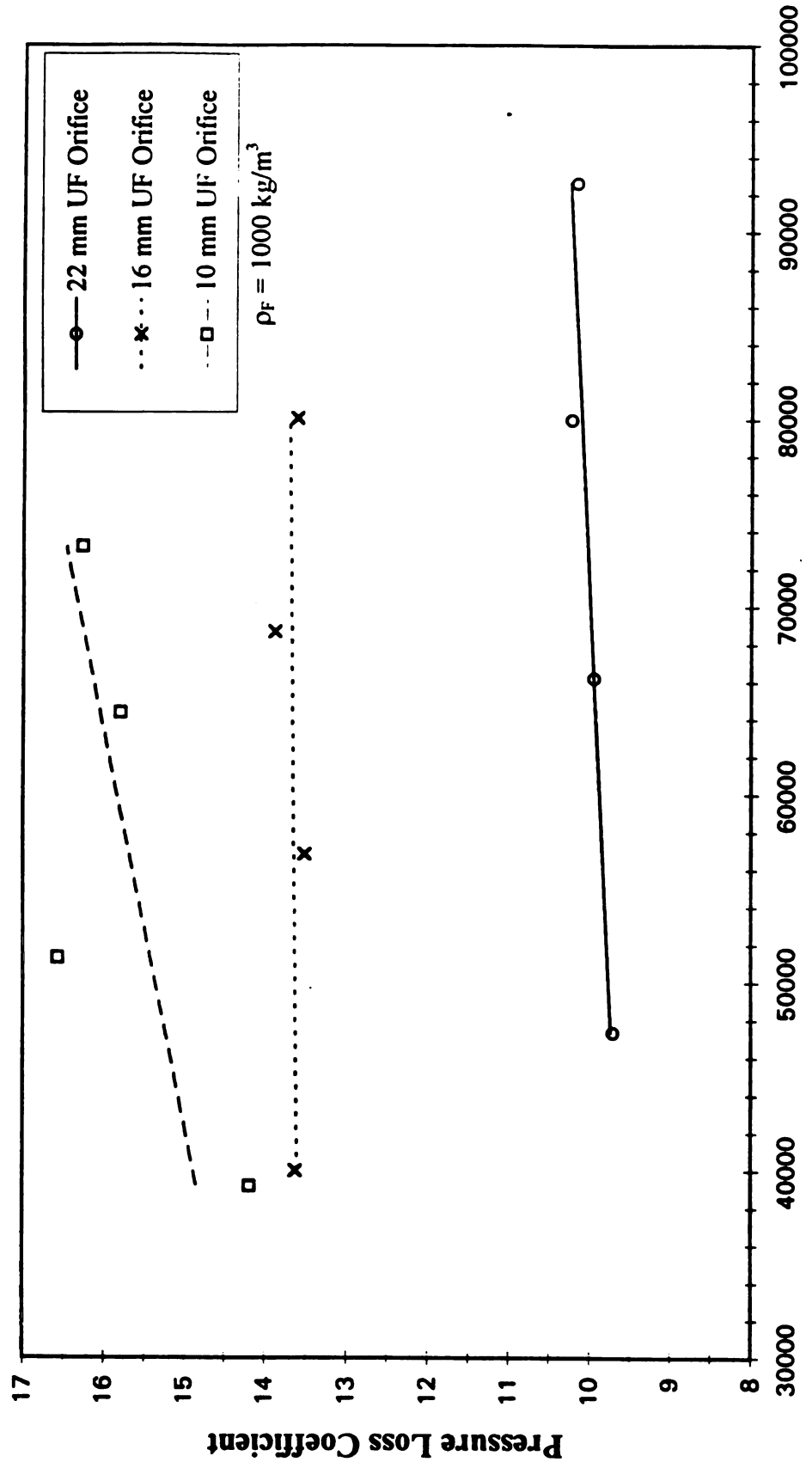

Figure 23: Pressure Loss Coefficient as a Function of Reynolds Number for the 20° Hydrocyclone

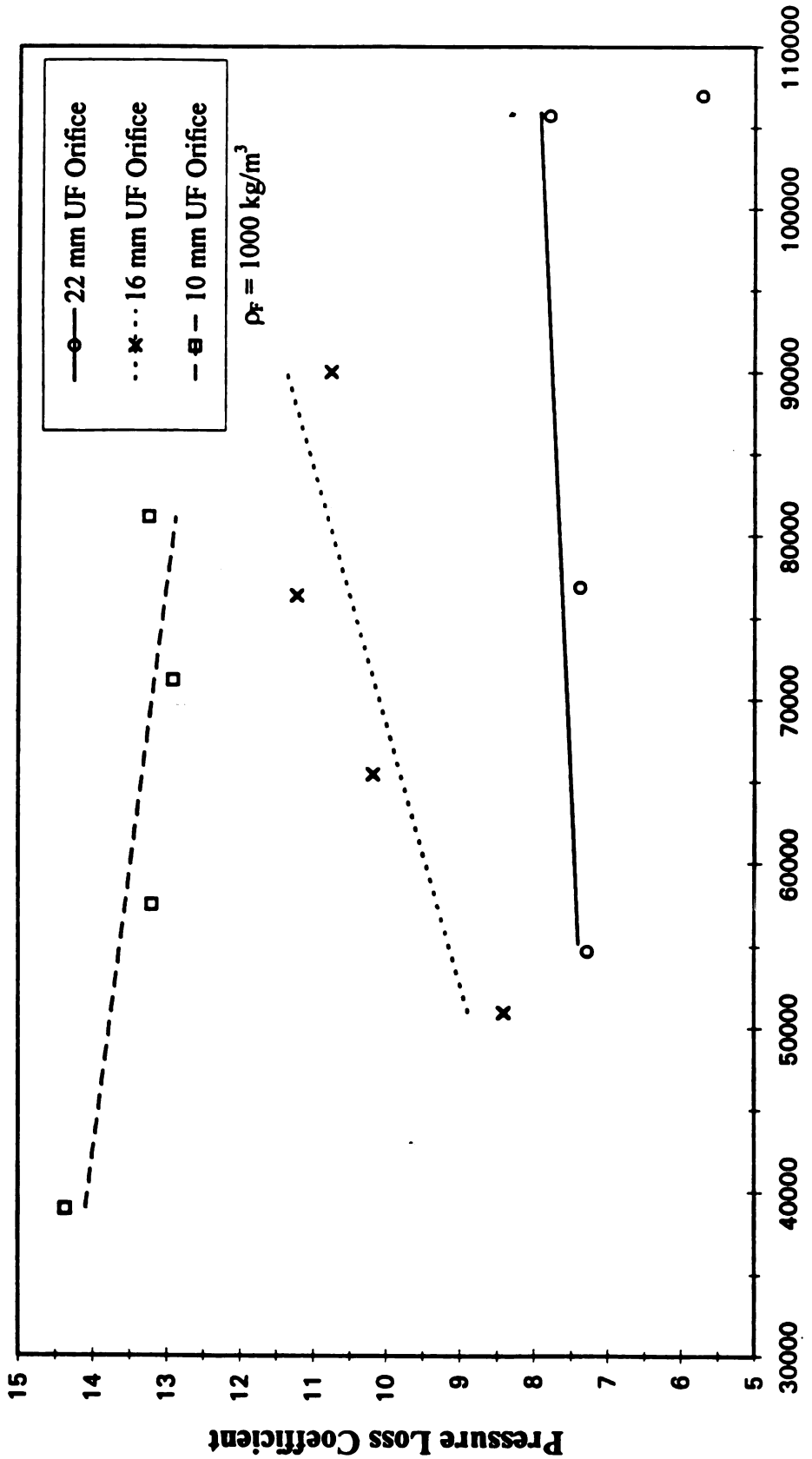

Figure 24: Pressure Loss Coefficient as a Function of Reynolds Number for the 10° Hydrocyclone

4.2 Stability of Microbubble Suspension

Migration of Microbubbles

A density gradient of microbubbles is established in the hydrocyclone because of microbubble migration relative to the continuous phase. Depending on the local density of the PP/HDPE separation zone, the HDPE and/or PP may appear either heavy or light and, thereby, report to either the underflow or the overflow. Figure 25 shows how the yield and underflow density change as a function of inlet density. The yield does not increase significantly until the underflow density approaches the density of HDPE. When the underflow density equals 960 kg/m^3, the HDPE becomes mutually buoyant and has a 50-50 chance of reporting to either the underflow or overflow. As the underflow density decreases further, the yield of HDPE increases significantly, however, the amount of PP reporting to the underflow stream begins to increase as ρ_U approaches 910 kg/m^3. The purity of the underflow stream drops sharply as ρ_U decreases below the density of PP. Clearly, high yields of HDPE at relatively high purities can be achieved in the LMH for underflow densities which satisfy the following inequality:

$$\rho_F < \rho_{PP} < \rho_U < \rho_{HDPE}.$$

This inequality explains why such low feed densities are needed for the Krebs hydrocyclone. It is noteworthy that for a dense medium operation, the separation occurs at a higher density than the feed density (see p.171 Bradley, 1965). Apparently this occurs because the migration of the medium is favorable to the

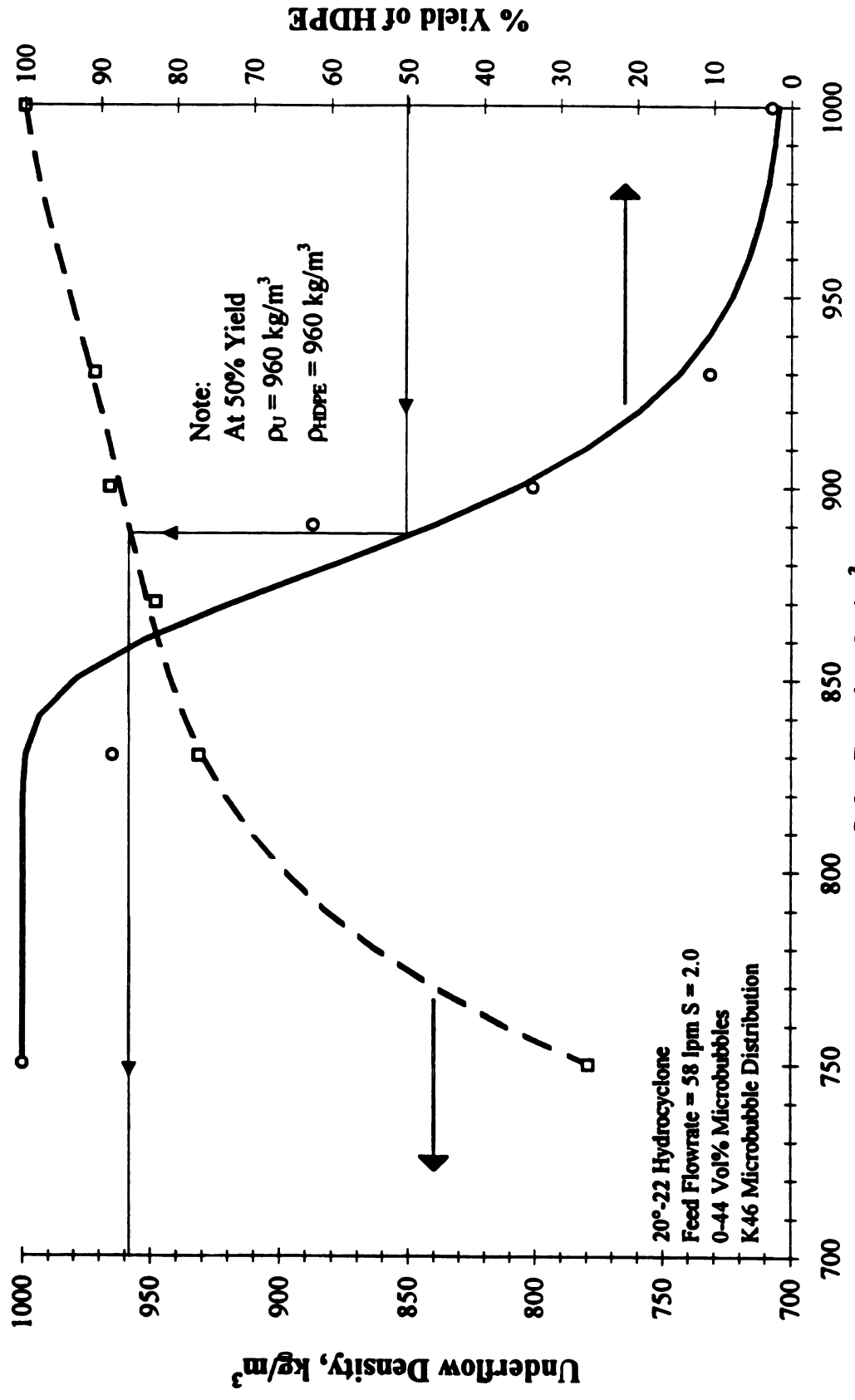

Figure 25: Yield and Underflow Density at Different Inlet Densities

separation. In the LMH, however, the migration of the medium is apparently unfavorable to the separation inasmuch as the underflow density is always higher than the feed density and the overflow density is always lower than the feed density.

The fundamental distinction between a dense medium and a light medium cyclone is the relative motion of the medium in the swirling flow field. Glass microbubbles tend to migrate towards the air core in a LMH whereas magnetite particles tend to migrate towards the conical wall in a DMH. Perhaps an improved LMH design could be developed based on the unique features of the light medium with the result that

$$\rho_{PP} < \rho_{HDPE} < \rho_F < \rho_C.$$

The overflow density, ρ_O, can be related to the feed density, underflow density, and split ratio by using a steady-state material balance (see Eq.(2)):

$$\rho_O = (\rho_F - \rho_U) \cdot S + \rho_F \qquad (24)$$

For ρ_F = 830 kg/m^3, ρ_U = 970 kg/m^3, and S = 2.0, Eq. (24) implies that ρ_O = 550 kg/m^3. This density is low and poses a large barrier for the migration of PP toward the vortex core. An overflow density of 550 kg/m^3 corresponds to a microbubble concentration of 57 vol.%. Thus, approximately 87% of the microbubbles in the feed are reporting to the overflow. This is a significant separation of the

microbubbles, and implies that only a small fraction of the microbubbles (≈ 13%) may be participating in the separation of HDPE and PP. Clearly, further control of the migration of microbubbles within the LMH could provide improvements in performance.

Microbubble Break-Up

Figure 15 shows that the high shear centrifugal pump environment breaks the microbubbles to a larger extent than the low shear progressive cavity pump. The sharp rise and tapering off of the cumulative breakage curve suggests that the centrifugal pump quickly breaks the weak microbubbles. The stronger microbubbles are more resistant to the high shear environment and take a longer exposure time to break in the shear pump. In contrast, the low shear environment of the progressive cavity pump gradually breaks the weak microbubbles resulting in the lower break-up rate shown in Figure 15.

The short time breakage data summarized by Figure 15 does not show a plateau for either pump. However, the long time experiment in the progressive cavity pump (see Figure 16) seems to suggest that a residual amount of microbubbles are resistant to breakage. This suggests that the microbubbles could be preprocessed to remove the weak ones and that the remaining strong microbubbles could be used in a process indefinitely. Therefore, fresh microbubbles would have to be

added to make up only for losses from the microbubble recovery system, not from breakage. This observation may influence the practical application of the proposed LMH for separating HDPE and PP.

Another aspect of the strength of the microbubbles is their use for short-time processing. The behavior of the microbubbles to withstand periods in which they are not suspended and allowed to dry is important. When the microbubbles float to the water/air interface, they tend to dry out. It is thought that this drying process may cause stress fractures on the microbubble surface resulting in a weaker product. These weakened microbubbles are then more susceptible to breaking up in the pump. The linear breakage rate portrayed by the data of Figure 16 suggests this effect. The microbubbles on the second day showed a higher amount of breakage, and consequently, may imply that the drying process damaged the microbubbles. Unlike the earlier portion of the curve, the breakage curve does not taper off after four hours of operation. This phenomena suggests that the microbubbles should remain wet whenever the flow is interrupted.

4.3 Separation Performance

The separation performance curves presented in Chapter 3 show that the yield and purity could be correlated with the dimensionless inlet density, ρ_F/ρ_{50}. The cut-density ρ_{50} is the feed density for which the recovery of HDPE in the underflow is

50% (i.e., $E_1(1) = 0.50$). Eq.(19) was found to be a useful empirical representation of $E_1(\rho_F/\rho_{50})$ with $b \approx 20$ for all the variations in design and operating conditions examined.

It is noteworthy that at ρ_{50}, $\rho_U = \rho_{HDPE}$ for the specific cyclone design and operating conditions studied. A desirable goal, albeit not attainable with the current design, is for $\rho_{50} > \rho_{HDPE}$.

Effect of Split Ratio on ρ_{50}

The split ratio affects the amount of medium needed for a given separation. For dense medium hydrocyclones, less material is needed when the underflow to overflow volumetric ratio is high. This same trend was observed in the light medium hydrocyclone. The values of ρ_{50} for S=0.1 and 0.6 were 660 and 750 kg/m^3, respectively. This means that a large amount of microbubbles are needed to achieve the proper underflow density for separation. Apparently, when the microbubbles enter the system and begin to separate, a large portion are caught in the strong upward flow and never participate in the separation. To counter this effect, more microbubbles are needed to achieve the proper underflow concentration for separation. Conversely, at higher split ratios the migration of microbubbles to the overflow decreases. Figure 26 shows graphically how ρ_{50} changes for the 20° hydrocyclone with three different underflow fittings. The

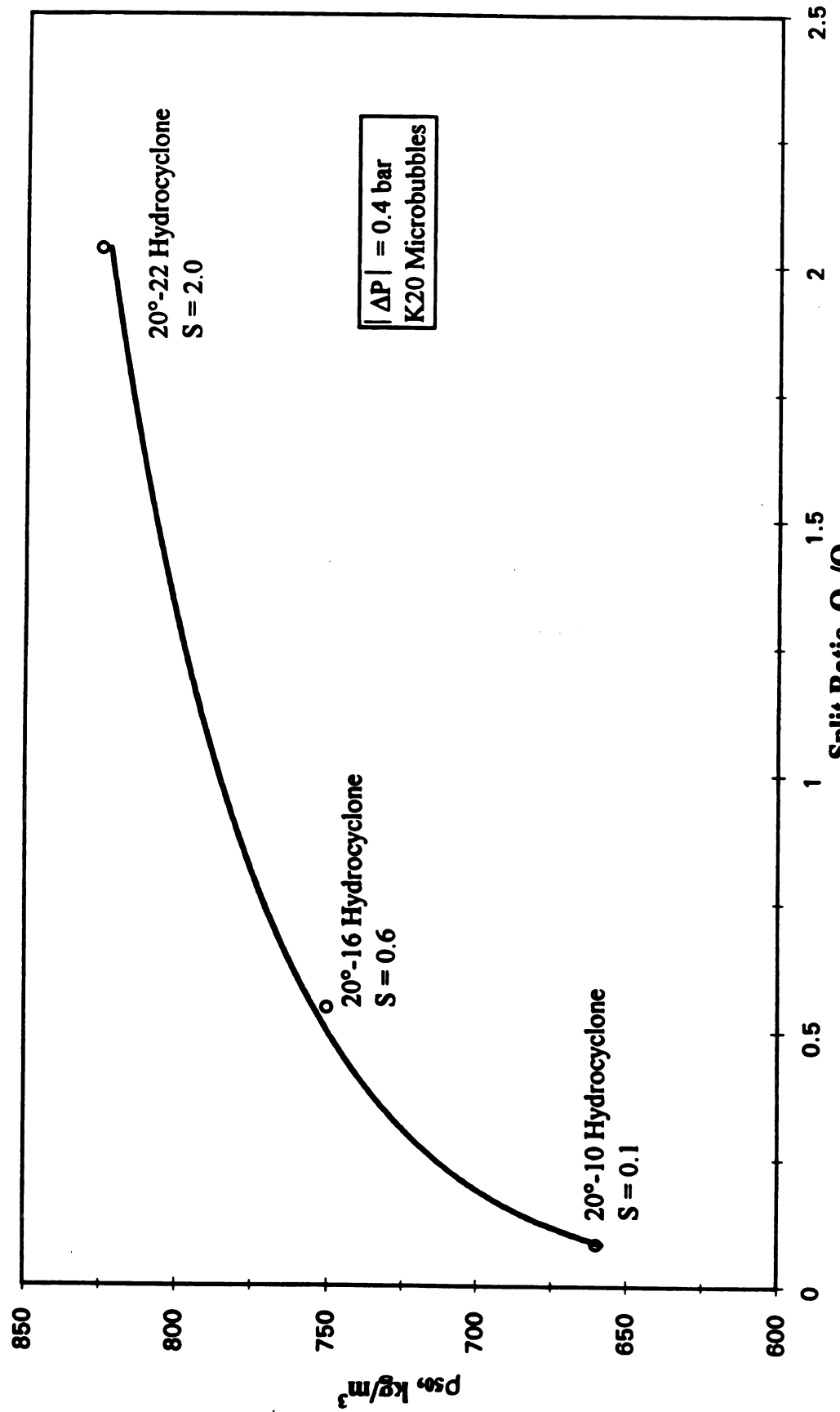

Figure 26: ρ_{50} as a Function of Split Ratio

figure shows that ρ_{50} increases significantly for split ratios below one, but then increases less rapidly for split ratios above one. This implies that there may be a practical upper limit on the ratio of D_U/D_O.

Effect of Feed Flow Rate on ρ_{50}

ρ_{50} increases with the feed flow rate, Q_F, because the centrifugal acceleration, $\langle u_\theta \rangle^2/r$, is proportional to Q_F^2. If the tangential velocity is proportional to the feed velocity, then the centrifugal acceleration for the higher flow rate is clearly larger than it is for the lower feed flow rate at any given radius. This increases the migration of the microbubbles to the core of the hydrocyclone, resulting in a lower concentration in the underflow. Again, more microbubbles are needed to attain the proper underflow density. As stated earlier, the split ratio also slightly decreased from 2.0 to 1.7 at the higher flow rate. Using Figure 26, the differences of ρ_{50}'s due to the change in split ratio is 15 kg/m^3 (830 down to 815 kg/m^3). The experimental values for the two flow rates are 830 kg/m^3 at 58 lpm and 780 kg/m^3 at 81 lpm. This is a difference of 50 kg/m^3 and shows that the increase in centrifugal acceleration is more dominant than the decrease in split ratio for these conditions. Consequently, feed flow rate (velocity) is an important parameter because of its influence on the centrifugal acceleration.

Effect of Microbubble Distribution on ρ_{50}

The smaller size microbubble distribution (K46) provided better performance than the K20 distribution inasmuch as the yield of HDPE was higher for a given feed density at the same flow rates and split ratios. The values of ρ_{50} were determined to be 830 kg/m^3 for the K20 distribution and 870 kg/m^3 for the K46 distribution. It appears that the K46 microbubbles provide a more stable medium. This was anticipated because of the lower drift velocity for the K46 distribution. Which is approximately one-fourth of the drift velocity for the K20 microbubble distribution (see Section 2.1).

Effect of Cone Angle on ρ_{50}

The cone angle seems to have the smallest effect on the yield of HDPE in the underflow of any of the parameters discussed. The 10°-22 hydrocyclone has a higher ρ_{50}, 880 kg/m^3, than the 20°-22 hydrocyclone, 860 kg/m^3, at the same inlet flow rate (67 lpm) and split ratio (1.8). This result was anticipated from the literature on dense medium separations and is attributed to a more active toroidal recirculation zone (TRCZ) in the 20°-22 hydrocyclone (Moder, 1952). In the 20° configuration, the microbubbles which are in the lower portion of the hydrocyclone can be caught in the TRCZ which would increase the microbubbles chances of reporting to the overflow. This is less likely to occur in the 10°

hydrocyclone because of the less active TRCZ. The small difference in the ρ_{50}'s for the two hydrocyclones is due the fact that the cone angles are not that great.

Effect of HDPE Concentration

In dense medium separations, the amount of solids does not affect the performance of the hydrocyclone up to concentrations of 4 wt.% (Moder, 1952). This also appears to be true in the light medium hydrocyclone, but the concentrations studied are well below the DMH concentrations. As stated in Chapter 2, the centrifugal pump would not function with plastic concentrations above 0.5 wt.%. Even though the concentrations are low, the results are still encouraging.

The fact that the concentration of HDPE did not have an effect on the recovery of HDPE in the underflow is very important to the application of this process. If this fact holds for high plastic loadings then this would greatly reduce the amount of medium necessary for separation. However, the effect of plastic concentration needs to be further researched to determine how the purity of the underflow stream is affected, and to determine at what concentration the yield begins to decrease.

CHAPTER 5

CONCLUSIONS AND ENGINEERING SIGNIFICANCE

Polypropylene and High Density Polyethylene can be separated in a hydrocyclone using a suspension of glass microbubbles in water. However, the separation of these two materials in a hydrocyclone is much more complicated than a float/sink tank. The migration of the microbubbles to the core is not advantageous to the separation, so more microbubbles are needed than the amount which would be calculated for a float/sink operation. Consequently, the suspension density of the feed stream to the hydrocyclone must be lower than either plastics for an effective separation (high yield, high purity). This study also shows that the underflow density, not the feed density, is the important factor in the separation of PP and HDPE, and that the inequality, $\rho_{PP} < \rho_U < \rho_{HDPE}$, must be satisfied for an effective separation of PP and HDPE.

The operating variables such as split ratio (Q_U/Q_O), flow rate (Q_F), cone angle (α), and microbubble size distribution affect the yield of HDPE in the light medium. These parameters influence the separation through concentration of microbubbles in the underflow stream. The higher this concentration, the higher the yield (i.e. E_1). The best combination of these variables for the operation of the reverse flow

hydrocyclone is: high split ratios, low inlet velocities, small cone angle, and small microbubbles. These conditions will provide the highest yield at the lowest inlet density, but may not be the best in terms of productivity. Figure 27 shows that for the 20°-22 hydrocyclone the separation efficiency, E, is a maximum for $\rho_F/\rho 50 = 0.96$.

Also, it was shown that the similarity hypothesis, $E_1(\Phi_F, Re_F) \rightarrow E_1(\rho_F/\rho_{50}^{(1)})$, appears to be valid, and that the effect of the hydrocyclone design and operating parameters are expressed in Eq. (19) through dependence of the recovery coefficient on ρ_{50}. Furthermore, it appears that the parameter b, which reflects the sharpness-of-separation, is insensitive to the operating conditions and hydrocyclone geometry with an approximate value of 20.

Finally, the reverse flow hydrocyclone may not be the best design for separating HDPE and PP. The 100 mm hydrocyclone which was used in these experiments was designed for dense medium separators. Table 5 is a comparison of the light medium and dense medium separations. It shows that the behavior of the two processes are similar in some respects and opposite in others. The most important difference being the amount of suspended material needed for separation. The dense medium hydrocyclone takes advantage of the medium's migration and,

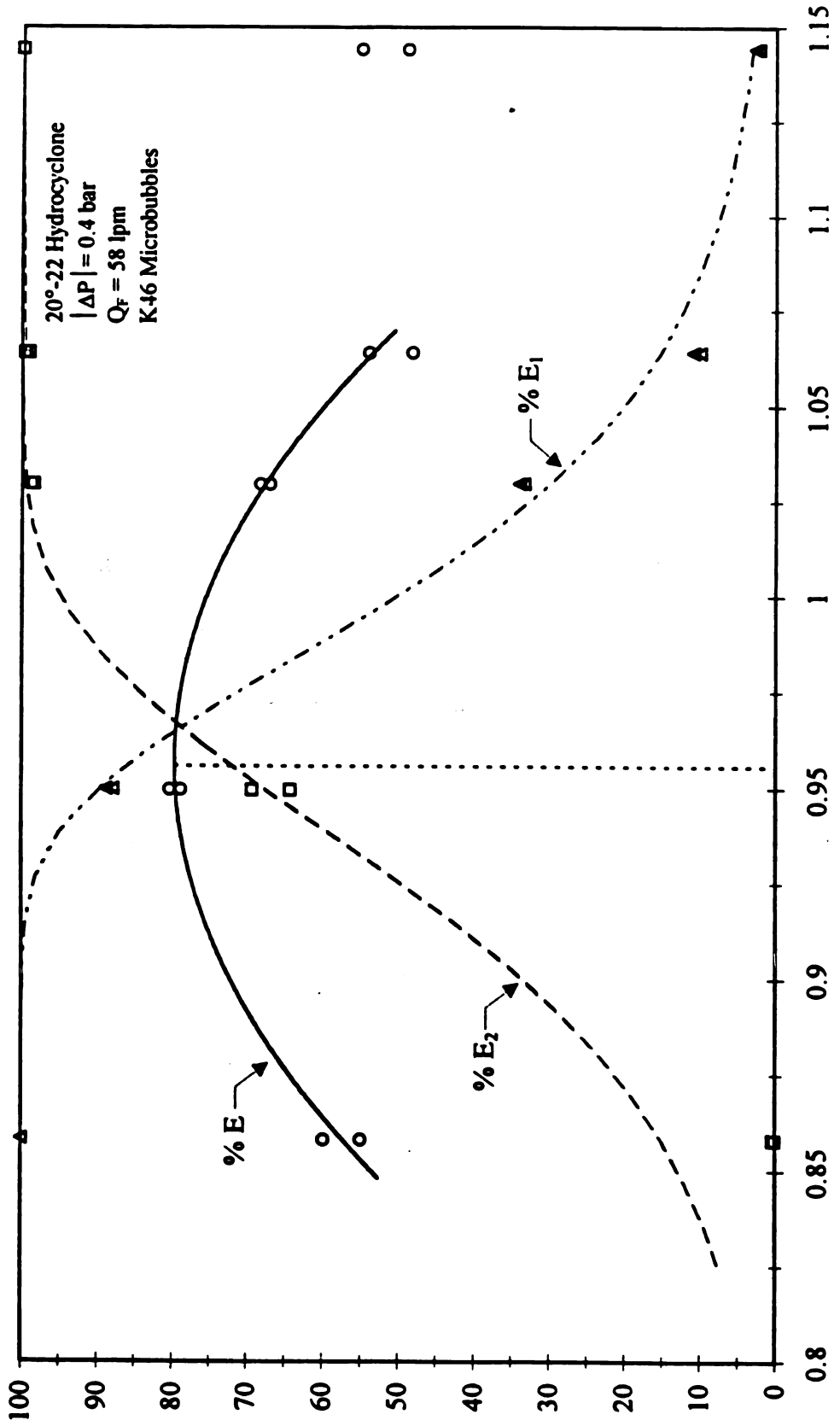

Figure 27: Separation Performance in the LMH

Table 5: Comparison of Light Medium Hydrocyclone and Dense Medium Hydrocyclones

Parameter	Effect on DMH	Effect on LMH
Amount of material in system	Less than amount calculated for float/sink tank	Higher than amount calculated for float/sink tank
Increase split ratio	Decrease amount of medium needed for separation	Decrease amount of medium needed for separation
Increase flow rate	Decrease amount of medium needed for separation	Increase amount of medium needed for separation
Decrease cone angle	Decrease amount of medium needed for separation	Decrease amount of medium needed for separation

consequently, uses less material than the amount calculated for a float/sink operation. In the LMH, however, the migration of the microbubbles is not advantageous, resulting in the use of more microbubbles than what is calculated in order that the density be between the densities of PP and HDPE. It is for this reason that the reverse flow hydrocyclone may not be suitable for separating HDPE and PP.

Engineering Significance

The yield/purity curves (see Figures 18-21) allows for an estimation of the flows in the process on the basis of a specific operating point. Figure 28 is a schematic for a process to produce a clean stream of HDPE. This flow diagram was constructed to process a feed stream from a typical reclamation facility. The flow rate of the feed stock was quoted from Michigan Polymer Reclaim (MPR) which is a HDPE recycling facility in Lansing, MI which uses float/sink technology to separate heavy contaminants from light thermoplastic materials. MPR produces approximately 1000 lbs. of HDPE per hour (7.6 kg/min) containing about 1 wt.% PP. The following hypothetical example calculation identifies an LMH process which reclaims an HDPE product containing 0.2 wt.% PP.

In order to calculate the stream variables, it was assumed that the performance of the LMH was independent of thermoplastic concentration (up to 4 wt.%), and that

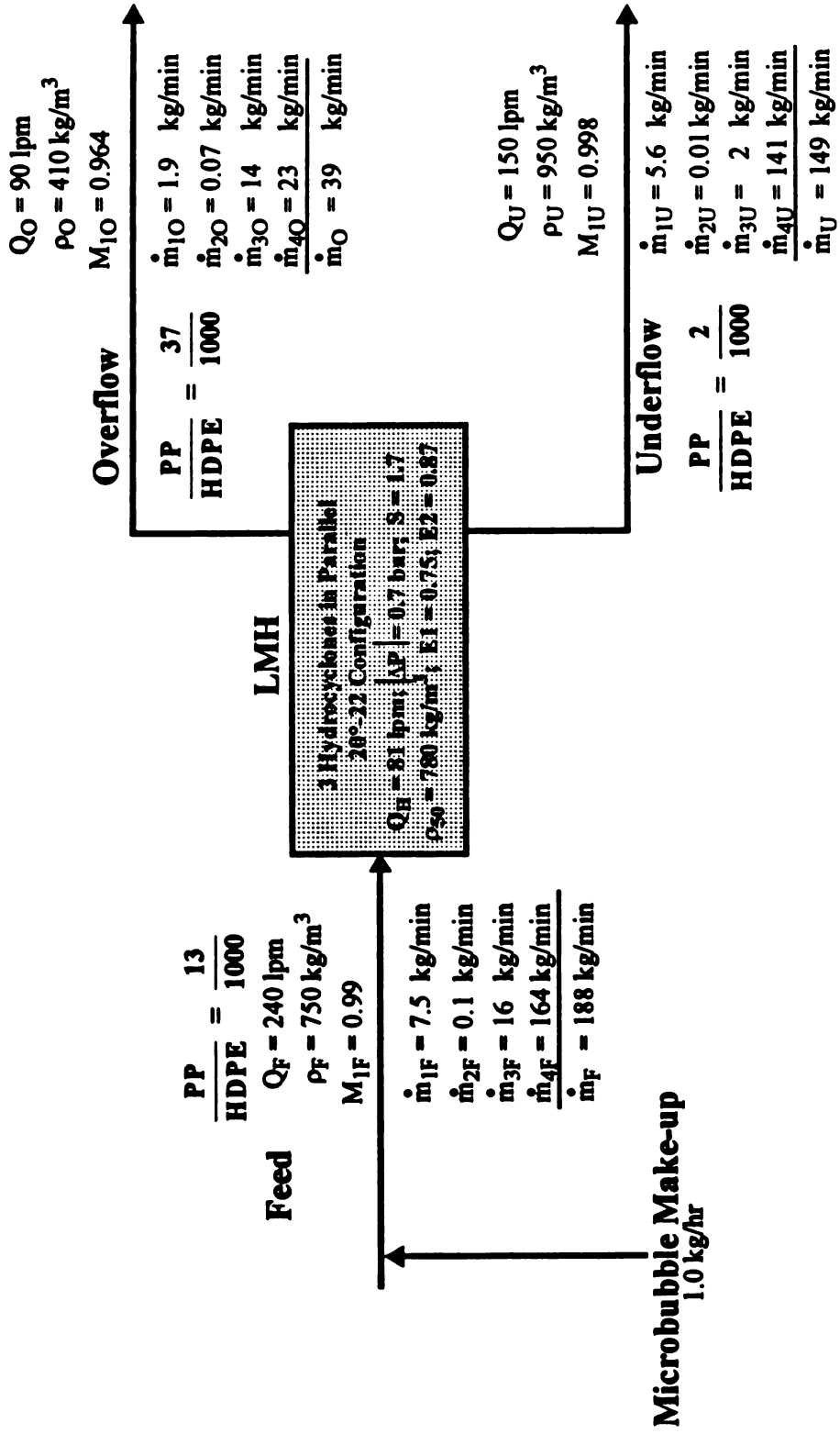

Figure 28: Flow Diagram for a Light Medium Hydrocyclone

the loss of medium for the process was 2 kg per ton of treated material as is the case in dense medium separations (see p. 21-33, Perry's, 1984). Also, it was assumed that the microbubbles did not break in the flow circuit.

For these calculations, the 20°-22 hydrocyclone configuration was chosen because it had the highest flow rate of the hydrocyclones which were studied. The flow rate for this configuration is 81 lpm at a pressure drop of 0.7 bar. A reduced inlet density of 0.96 was chosen because of the high yield and high purity (see Figure 19). This reduced inlet density corresponds to an actual feed density of 750 kg/m^3. At the specified flow rates of the thermoplastics, 240 lpm of feed suspension is required. To meet the flow requirements of the facility, 3 hydrocyclones operating in parallel are needed. The performance data from Figure 19 shows a HDPE recovery in the underflow of 75% and a corresponding stream purity of 85%. This coincides to approximately 87% PP recovery in the overflow stream.

Figure 28 shows the conditions of all process streams. The important factors to note are the HDPE stream purity coefficients, M_{1x}, the stream densities, and the relative amount of PP to HDPE. The stream purity coefficient is 0.99 for the inlet stream to the hydrocyclone assembly. It is increased to 0.998 in the underflow stream by passing it through the LMH. The overflow stream purity, however, has been decreased to 0.964. The overflow stream may be further processed to

improve its purity and also to increase the yield of HDPE for the entire process. The ratios of PP to HDPE in every stream are quite low. However, the flow diagram shows that the grade of HDPE in the underflow is improved significantly. Figure 28 shows an anticipated decrease in the mass ratio of PP to HDPE by a factor of seven.

As stated earlier, the underflow density controls the recovery of HDPE in the LMH. Therefore, because of similarity in the yield/purity curves, the yield for different operating parameters can be predicted for a given underflow density. Following this logic, the underflow density was determined from Figure 24 to be 950 kg/m^3. Using the feed and underflow densities, along with a split ratio of 1.7, the overflow density was calculated to be 410 kg/m^3. To further utilize the overflow in the separation process, it would be necessary to add water to increase the overflow density.

CHAPTER 6

RECOMMENDATIONS FOR FURTHER STUDY

The following recommendations for further study with the current light medium hydrocyclone are made:

1. Perform flow visualization experiments on the LMH. The setup of the LMH would not allow the separation of PP and HDPE to be viewed. An understanding of where the separation is occurring in the hydrocyclone may provide insight into the design of new hydrocyclones for this application. This entails more than just making a clear hydrocyclone and viewing the HDPE and PP. The microbubbles make the suspension opaque, even in small concentrations. Consequently, the continuous phase will have to be made optically homogeneous by adding a soluble constituent to the water in order to match the refractive indices of the water and the microbubbles.

2. Perform more experiments with the current light medium flow circuit to fill in the areas which were not covered in this research. It is suggested that experiments be conducted at higher flow rates using lower feed densities. Also, experiment with different cone angles and microbubbles size distributions. Since ρ_{50} is a function of the design and operating parameters, a

more detailed study of the dependence of ρ_{50} on the hydrocyclone geometry and feed conditions is needed in order to perform any significant engineering calculations. Also, further study may indicate if b is a function of any of the experimental conditions.

3. A more detailed study of the microbubble breakup may be helpful. This may indicate how the microbubbles break in the system and how to manufacture microbubbles which are more resistant to breaking. Also, from an economic point of view, it would be important to know if there is an upper limit to the amount of breakage.

4. Try to effect the size and shape differences in HDPE and PP via grinding protocol. Table 2 showed that there are significant temperature differences in the thermal transitions of PP and HDPE. Also, HDPE is difficult to fracture at cryogenic temperatures while PP is easier. Depending on the conditions (temperature, impact rate, residence time), it may be possible to obtain differences in size and or shape of the particles. Dreissen et al. (1963) have shown that shape can be a major factor in the separation of particles with similar densities. This may lead to an autogeneous (water only) design, or at least decrease the amount of microbubbles necessary for separating PP and HDPE.

5. Experiment with completely different hydrocyclones. As stated in Chapter 5, the reverse flow hydrocyclone may not be the best design for this separation because the microbubbles are quickly removed in the overflow stream. A hydrocyclone with a totally different flow pattern, such as a forward flow hydrocyclone, may decrease the migration to the overflow. Alternatively, the migration of the microbubbles may be decreased by increasing the length of the vortex finder (See Figure 1). This would provide a physical barrier to the migration of the microbubbles to the vortex, thereby increasing the concentration of microbubbles in the apex region of the hydrocyclone.

APPENDIX A

HYDRAULIC DATA

Table A.1: Flow Rate/Pressure Drop Data for the 20° Hydrocyclone

V_H = .7 gallons

10 mm Underflow Orifice Inlet Pressure (psi)	UF (gpm)	OF (gpm)	Feed* (gpm)	UF/F	OF/F	UF/OF	Feed Vel. (ft/s)	Feed Vel. (m/s)	Mean Residence Time (sec)
5	0.98	11.66	12.64	0.08	0.92	0.08	7.23	2.20	10.46
10	1.00	15.54	16.54	0.06	0.94	0.06	9.46	2.88	10.46
15	1.09	19.66	20.75	0.05	0.95	0.06	11.87	3.62	10.46
20	1.17	22.44	23.61	0.05	0.95	0.05	13.51	4.12	10.46

16 mm Underflow Orifice Inlet Pressure (psi)	UF (gpm)	OF (gpm)	Feed* (gpm)	UF/F	OF/F	UF/OF	Feed Vel. (ft/s)	Feed Vel. (m/s)	Mean Residence Time (sec)
5	4.55	8.35	12.90	0.35	0.65	0.54	7.38	2.25	10.46
10	6.17	12.15	18.32	0.34	0.66	0.51	10.48	3.20	10.46
15	7.24	14.90	22.14	0.33	0.67	0.49	12.67	3.86	10.46
20	8.37	17.45	25.82	0.32	0.68	0.48	14.77	4.50	10.46

22 mm Underflow Orifice Inlet Pressure (psi)	UF (gpm)	OF (gpm)	Feed* (gpm)	UF/F	OF/F	UF/OF	Feed Vel. (ft/s)	Feed Vel. (m/s)	Mean Residence Time (sec)
5	10.24	5.04	15.28	0.67	0.33	2.03	8.74	2.66	10.46
10	13.52	7.83	21.35	0.63	0.37	1.73	12.22	3.72	10.46
15	16.26	9.53	25.79	0.63	0.37	1.71	14.76	4.50	10.46
20	18.69	11.18	29.87	0.63	0.37	1.67	17.09	5.21	10.46

*** determined by steady state material balance**

Table A.2: Flow Rate/Pressure Drop Data for the 10° Hydrocyclone

V_H = 0.7 gallons

10 mm Underflow Orifice

Inlet Pressure (psi)	UF (gpm)	OF (gpm)	Feed* (gpm)	UF/F	OF/F	UF/OF	Feed Vel. (ft/s)	Feed Vel. (m/s)	Mean Residence Time (sec)
5	1.35	11.21	12.56	0.11	0.89	0.12	7.19	2.19	10.46
10	1.45	17.08	18.53	0.08	0.92	0.08	10.60	3.23	10.46
15	1.55	21.40	22.95	0.07	0.93	0.07	13.13	4.00	10.46
20	1.59	24.58	26.17	0.06	0.94	0.06	14.97	4.56	10.46

16 mm Underflow Orifice

Inlet Pressure (psi)	UF (gpm)	OF (gpm)	Feed* (gpm)	UF/F	OF/F	UF/OF	Feed Vel. (ft/s)	Feed Vel. (m/s)	Mean Residence Time (sec)
5	6.77	9.65	16.42	0.41	0.59	0.70	9.40	2.86	10.46
10	8.33	12.77	21.10	0.39	0.61	0.65	12.07	3.68	10.46
15	9.29	15.33	24.62	0.38	0.62	0.61	14.09	4.29	10.46
20	11.19	17.84	29.03	0.39	0.61	0.63	16.61	5.06	10.46

22 mm Underflow Orifice

Inlet Pressure (psi)	UF (gpm)	OF (gpm)	Feed* (gpm)	UF/F	OF/F	UF/OF	Feed Vel. (ft/s)	Feed Vel. (m/s)	Mean Residence Time (sec)
5	11.51	6.14	17.65	0.65	0.35	1.87	10.10	3.08	10.46
10	15.80	8.99	24.79	0.64	0.36	1.76	14.18	4.32	10.46
15	22.35	12.16	34.51	0.65	0.35	1.84	19.75	6.02	10.46
20	20.69	13.42	34.11	0.61	0.39	1.54	19.52	5.95	10.46

* determined by steady state material balance

APPENDIX B

MEDIUM STABILITY DATA

Table B.1: Average Density of Glass Microbubbles

K - 20 MICROBUBBLES

TRIAL #	DENSIT (kg/m^3)	BULK ENSITY (kg/m^3)
1	317	70
2	173	51
3	225	88
4	187	98
5	167	84
AVE	214	78
ST. DEV	62	18

K-46 MICROBUBBLES

TRIAL #	DENSIT (kg/m^3)	BULK ENSIT (kg/m^3)
1	500	250
2	455	221
3	387	212
4	413	207
5	467	240
AVE	444	226
ST. DEV	45	18

Table B.2: Size Distribution for the K20 Microbubbles

Determined Using a Malvern Mastersizer

l_{50}= 51.57

Size microns	% Under	Size microns	% Under
0.5	0.50	9.94	2.90
0.55	0.60	10.9	3.30
0.6	0.70	12	3.70
0.66	0.80	13.2	4.20
0.73	0.90	14.4	4.70
0.8	1.00	15.9	5.40
0.88	1.10	17.4	6.30
0.96	1.10	19.1	7.40
1.06	1.10	21	8.70
1.16	1.20	23	10.30
1.27	1.20	25.3	12.40
1.4	1.20	27.8	14.90
1.53	1.20	30.5	17.90
1.68	1.20	33.5	21.60
1.85	1.20	36.8	26.20
2.03	1.20	40.4	31.60
2.23	1.20	44.3	37.80
2.45	1.20	48.7	45.00
2.69	1.30	53.4	53.10
2.95	1.30	58.7	61.60
3.24	1.30	64.4	69.70
3.56	1.30	70.7	77.20
3.91	1.40	77.6	83.60
4.29	1.40	85.2	88.30
4.71	1.50	93.6	92.00
5.17	1.60	103	94.90
5.67	1.70	113	96.80
6.23	1.80	124	98.00
6.84	2.00	136	98.80
7.51	2.20	149	99.30
8.25	2.40	164	99.70
9.05	2.70	180	100.00

Table B.3: Size Distribution for the K46 Microbubble

Determined Using a Malvern Mastersizer

t_{50}= 32.1

Size microns	% Under	Size microns	% Under
0.5	1.1	9.94	7.1
0.55	1.4	10.9	8.5
0.6	1.7	12	10.1
0.66	1.9	13.2	11.9
0.73	2.1	14.4	14.1
0.8	2.3	15.9	16.6
0.88	2.4	17.4	19.4
0.96	2.6	19.1	22.6
1.06	2.6	21	26.3
1.16	2.7	23	30.5
1.27	2.7	25.3	35.3
1.4	2.8	27.8	40.7
1.53	2.8	30.5	46.6
1.68	2.8	33.5	53
1.85	2.8	36.8	59.7
2.03	2.8	40.4	66.5
2.23	2.8	44.3	72.9
2.45	2.8	48.7	78.9
2.69	2.9	53.4	84
2.95	2.9	58.7	88.3
3.24	2.9	64.4	91.6
3.56	2.9	70.7	94
3.91	3	77.6	95.8
4.29	3.1	85.2	97.1
4.71	3.2	93.6	98
5.17	3.3	103	98.6
5.67	3.5	113	99.1
6.23	3.8	124	99.4
6.84	4.1	136	99.6
7.51	4.6	149	99.7
8.25	5.3	164	99.9
9.05	6.1	180	100

Table B.4: Medium Separation Data

K20 Microbubble Distribution

Cone =	20°-22	20°-22	20°-22	20°-22
	5 psi	7.5 psi	10 psi	20 psi
Inlet	Underflow	Underflow	Underflow	Underflow
Density	Density	Density	Density	Density
(kg/m^3)	(kg/m^3)	(kg/m^3)	(kg/m^3)	(kg/m^3)
1000	100	100	1000	1000
900	980	990	990	
880	980	990	990	1000
830	970	980	980	990

K46 Microbubble Distribution

Cone =	20°-22	20°-22	10°-22
	5 psi	7 psi	5 psi
Inlet	Underflow	Underflow	Underflow
Density	Density	Density	Density
(kg/m^3)	(kg/m^3)	(kg/m^3)	(kg/m^3)
1000	1000	1000	1000
930	970	980	970
900	970	970	960
870	950	960	960
830	930	950	940

Table B.5: Glass Microbubble Break Different Pumps

Progressive Cavity Pump
(6% breakup new)

Time (Minutes)	Weight Broken (grams)	Weight Unbroken (grams)	% Broken
2	0.02	0.13	13.96
30	0.06	0.65	7.88
60	0.07	0.40	15.18
90	0.07	0.67	10.07
120	0.07	0.53	11.29
150	0.06	0.64	9.09
180	0.14	0.51	21.55
210	0.17	0.80	17.70
240	0.18	0.46	27.98

K20 Microbubbles
90 lpm

Centrifugal Pump
(6% breakup new)

Time (Minutes)	Weight Broken (grams)	Weight Unbroken (grams)	% Broken
2	0.09	0.24	27.60
30	0.24	0.22	52.41
60	0.16	0.60	20.69
90	0.32	0.31	50.36
120	0.30	0.59	33.86
150	0.27	0.48	35.73
180	0.38	0.53	41.37
210	0.27	0.39	41.13
240	0.31	0.53	36.55

K20 Microbubbles
20°-22 Hydrocyclone
90 lpm

Table B.6: Glass Microbubble Breakage

K20 Microbubble Volumetric Breakup
(2.6 % breakup new)

Time	Flowrat (lpm)	Temp (C)	Vol % Broke sample A	sample B	Avg
30	66	24.00	3.40	3.90	3.65
60	66	23.50	3.40	3.40	3.40
90	66	23.50	4.30	4.50	4.40
120	66	23.00	4.20	4.20	4.20
150	80	21.00	4.50	4.80	4.65
180	80	22.00	5.00	5.00	5.00
210	80	23.50	5.20	4.50	4.85
240	80	25.00	5.30	4.80	5.05
270	80	22.00	6.40	4.70	5.55

K20 Microbubble Volumetric Breakup
(Next Day)

Time	low rat (lpm)	Temp (C)	Vol % Broke sample A	sample B	Avg
270	66	23.00	6.40	6.40	6.40
300	66	23.00	5.56	6.34	5.95
330	66	23.00	6.47	6.59	6.53
360	66	22.00	7.37	7.14	7.26
390	66	23.00	7.19	7.98	7.58
420	66	23.00	7.51	7.19	7.35
450	94	24.00	8.57	7.61	8.09
480	94	22.00	8.82	9.06	8.94
510	94	22.00	8.54	8.98	8.76
540	94	22.00	9.09	10.98	10.04

APPENDIX C

SEPARATION PERFORMANCE DATA

Table C.1: HDPE/PP Particle Size Distribution

Sieve specifications:

tray no.	ASTM mesh	opening (mm)	opening (in)	tare wt. (g)
20	20	0.85	0.033	428.3
14	12	1.40	0.056	453.8
10	9	2.00	0.078	451.0
8	8	2.36	0.094	470.0
6	6	3.35	0.132	514.1
5	5	4.00	0.157	519.9

Size distribution of HDPE

Total Plastics (g)	Tray Number	Total Wt. Sieve (g)	Sieve Tare Wt. (g)	Wt.HDPE Tray (g)	Mass Undersize (g)
242.2	20	454.1	428.3	25.8	0.25
242.2	14	579.5	453.8	125.7	10.90
242.2	10	521.6	451.0	70.6	62.80
242.2	8	489.5	470.0	19.5	91.95
242.2	6	514.1	514.1	0.0	100.00
242.2	5	519.9	519.9	0.0	100.00

Size distribution of PP

Total Plastics (g)	Tray Number	Total Wt. Sieve (g)	Sieve Tare Wt. (g)	Wt.PP Tray (g)	Mass Undersize (g)
318.6	20	444.0	428.3	15.7	0.53
318.6	14	542.8	453.8	89.0	5.46
318.6	10	596.9	451.0	145.9	33.40
318.6	8	536.3	470.0	66.3	79.19
318.6	6	514.1	514.1	0.0	100.00
318.6	5	519.9	519.9	0.0	100.00

Table C.2: Data for the 20°-22 Hydrocyclone at 5 psi

K20 microbubbles
$|\Delta P| = 5$ psi (QF = 58 lpm)
sample time = 5 sec

Inlet Density (g/mL)	wt HDPE UF (g)	wt HDPE OF (g)	wt HDPE* Feed (g)	Wt PP UF (g)	wt PP OF (g)	wt PP* Feed (g)
1	0.026	1.208	1.234	0.000	3.057	3.057
	0.061	2.992	3.053	0.000	3.672	3.672
	0.025	0.451	0.475	0.000	2.225	2.225
0.95	0.069	2.681	2.749	0.082	2.736	2.818
	0.226	2.632	2.858	0.000	2.966	2.966
	0.300	2.447	2.747	0.000	2.741	2.741
0.925	0.405	2.482	2.887	0.085	1.850	1.935
	0.459	2.534	2.993	0.130	1.454	1.585
	0.322	2.450	2.772	0.079	1.897	1.976
0.9	0.324	3.511	3.835	0.027	1.300	1.327
	0.379	3.178	3.557	0.016	1.666	1.682
	0.390	3.169	3.559	0.031	1.410	1.441
0.875	0.374	3.043	3.416	0.075	2.855	2.930
	0.313	3.172	3.485	0.072	2.891	2.963
	0.375	2.741	3.116	0.065	2.671	2.736
0.875	0.448	2.656	3.104	0.147	3.013	3.160
	0.475	2.876	3.351	0.166	3.059	3.225
	0.607	3.106	3.713	0.184	3.003	3.187
0.85	1.059	2.318	3.377	0.014	2.404	2.417
	0.611	2.959	3.570	0.036	2.549	2.585
	0.567	2.649	3.216	0.009	2.522	2.531
0.825	1.884	2.005	3.889	0.410	3.454	3.864
	2.018	2.138	4.156	0.349	3.095	3.444
	2.798	3.004	5.803	0.242	3.056	3.299
0.825	2.616	2.271	4.886	0.287	4.353	4.640
	2.656	2.230	4.886	0.303	4.143	4.446
	2.105	2.195	4.300	0.426	5.382	5.808
0.825	3.452	2.440	5.892			
	2.916	2.402	5.318			
	3.272	2.427	5.699			
0.8	1.688	2.422	4.110	0.082	1.788	1.870
	1.884	2.294	4.178	0.147	3.521	3.668
	1.476	1.840	3.316	0.159	3.909	4.068
0.8	2.461	3.040	5.501	0.758	4.420	5.178
	2.260	2.710	4.970	0.690	4.030	4.720
	2.430	2.930	5.360	0.670	4.160	4.830
0.775	3.187	1.030	4.217	0.232	2.290	2.522
	3.120	1.000	4.120	0.244	4.000	4.244
	2.790	0.980	3.770	0.167	2.560	2.727
0.75	4.169	0.076	4.245	0.718	3.335	4.053
	3.687	0.153	3.839	0.409	2.971	3.380
	3.582	0.113	3.695	0.368	2.988	3.356
0.7	8.297	0.072	8.369	5.613	0.932	6.545
	7.785	0.060	7.845	5.382	1.434	6.816
	6.953	0.070	7.023	5.492	2.019	7.511

*determined by steady state material balance

Table C.3: Data for the 20°-22 Hydrocyclone at 10 psi

K20 microbubbles
$|\Delta P| = 10$ psi ($Q_F = 58$ lpm)
sample time = 5 sec

Inlet Density (g/mL)	wt HDPE UF (g)	wt HDPE OF (g)	wt HDPE* Feed (g)	Wt PP UF (g)	wt PP OF (g)	wt PP* Feed (g)
1	0.044	2.587	2.631	0.000	2.952	2.952
0.95	0.138	4.178	4.316	0.000	4.935	4.935
0.925	0.267	4.358	4.625	0.017	2.311	2.327
0.9	0.250	4.241	4.490	0.032	1.785	1.817
0.875	0.224	3.588	3.811	0.026	4.107	4.132
0.875	0.575	4.353	4.928	0.136	3.752	3.888
0.85	0.356	3.947	4.303	0.013	4.136	4.148
0.825	2.077	4.454	6.531	0.131	4.428	4.560
0.825	1.832	4.251	6.083	0.120	6.192	6.312
0.825	2.603	5.338	7.941			
0.8	1.720	4.290	6.010	0.360	5.630	5.990
0.8	1.386	3.394	4.780	0.111	3.880	3.991
0.775	2.330	3.970	6.300	0.065	4.030	4.095
0.75	3.927	0.671	4.598	0.408	5.050	5.457
0.7	8.861	0.550	9.411	3.246	5.700	8.946

*determined by steady state material balance

Table C.4: Data for the 20°-16 Hydrocyclone at 5 psi

K20 microbubbles
$|\Delta P| = 5$ psi ($Q_F = 58$ lpm)
sample time = 5 sec

Inlet Density (g/mL)	wt HDPE UF (g)	wt HDPE OF (g)	wt HDPE Feed (g)	Wt PP UF (g)	wt PP OF (g)	wt PP* Feed (g)
1	0.027	2.428	2.455	0.000	3.150	3.150
0.95	0.072	2.861	2.933	0.094	2.771	2.866
0.925	0.130	1.741	1.871	0.072	2.308	2.379
0.9	0.130	3.462	3.592	0.024	1.064	1.088
0.875	0.167	2.801	2.968	0.133	3.100	3.233
0.875	0.319	4.236	4.555	0.029	2.072	2.101
0.85	0.185	2.442	2.628	0.007	3.076	3.083
0.825	0.971	3.615	4.586	0.105	4.279	4.384
0.8	1.000	4.440	5.440	0.090	3.110	3.200
0.8	0.913	3.666	4.579	0.034	2.562	2.596
0.775	1.035	2.940	3.975	0.070	4.080	4.150
0.75	1.064	1.556	2.620	0.174	4.301	4.475

*determined by steady state material balance

Table C.5: Data for the 20°-16 Hydrocycloneat 10 psi

K20 microbubbles

$|\Delta P|$ = 10 psi (Q_F = 58 lpm)

sample time = 5 sec

Inlet Density (g/mL)	wt HDPE UF (g)	wt HDPE OF (g)	wt HDPE Feed (g)	Wt PP UF (g)	wt PP OF (g)	wt PP* Feed (g)
1	0.041	3.067	3.108	0.000	2.707	2.707
0.95	0.174	5.048	5.222	0.000	3.788	3.788
0.925	0.138	3.260	3.398	0.065	2.052	2.117
0.9	0.163	2.668	2.830	0.058	1.396	1.454
0.875	0.082	3.707	3.790	0.031	3.310	3.342
0.875	0.193	4.364	4.557	0.008	2.992	3.000
0.85	0.151	3.685	3.836	0.000	4.296	4.296
0.825	0.473	3.673	4.146	0.119	5.865	5.984
0.8	0.650	6.130	6.780	0.063	5.200	5.263
0.8	0.652	5.760	6.412	0.014	3.158	3.172
0.775	0.613	4.650	5.263	0.030	5.270	5.300
0.75	0.778	3.313	4.091	0.049	5.609	5.657

*determined by steady state material balance

Table C.6: Data for the 20°-10 Hydrocyclone at 5 psi

K20 microbubbles
$|\Delta P| = 5$ psi ($Q_F = 58$ lpm)
sample time = 5 sec

Inlet Density (g/mL)	wt HDPE UF (g)	wt HDPE OF (g)	wt HDPE Feed (g)	Wt PP UF (g)	wt PP OF (g)	wt PP* Feed (g)
1	0.006	1.483	1.489	0.000	2.426	2.426
0.95	0.000	4.722	4.722	0.000	2.209	2.209
0.925	0.000	2.424	2.424	0.046	2.198	2.244
0.9	0.018	2.222	2.239	0.019	1.414	1.433
0.875	0.000	3.341	3.341	0.000	2.239	2.239
0.875	0.014	4.471	4.485	0.000	1.754	1.754
0.85	0.000	2.891	2.891	0.000	2.893	2.893
0.825	0.071	3.596	3.666	0.022	3.242	3.264

*determined by steady state material balance

Table C.7: Data for the 20°-10 Hydrocyclone at 10 psi

K20 microbubbles
$|\Delta P|$ = 10 psi (Q_F = 58 lpm)
sample time = 5 sec

Inlet Density (g/mL)	wt HDPE UF (g)	wt HDPE OF (g)	wt HDPE Feed (g)	Wt PP UF (g)	wt PP OF (g)	wt PP* Feed (g)
1	0.000	2.848	2.848	0.000	3.406	3.406
0.95	0.000	6.301	6.301	0.000	3.082	3.082
0.925	0.027	3.847	3.873	0.020	2.172	2.192
0.9	0.023	2.602	2.625	0.024	1.113	1.137
0.875	0.000	2.514	2.514	0.000	3.265	3.265
0.875	0.000	6.012	6.012	0.000	2.733	2.733
0.85	0.000	2.900	2.900	0.000	4.000	4.000
0.825	0.042	3.573	3.614	0.229	3.953	4.182

*determined by steady state material balance

Table C.8: Data for the 20°-22 Hydrocyclone at 5 psi with K46 Microbubbles

Inlet Density (g/mL)	wt HDPE UF (g)	wt HDPE OF (g)	wt HDPE* Feed (g)	Wt PP UF (g)	wt PP OF (g)	wt PP* Feed (g)
1.00	0.110	4.705	4.815	0.000	5.597	5.597
	0.151	5.491	5.642	0.000	5.070	5.070
0.93	0.742	6.072	6.814	0.031	6.365	6.396
	0.762	6.820	7.582	0.055	5.592	5.647
0.90	2.223	4.342	6.565	0.115	7.280	7.395
	2.116	4.239	6.355	0.087	6.579	6.666
0.83	7.735	0.977	8.712	1.655	2.967	4.622
	7.114	0.984	8.098	2.384	5.365	7.749
0.75	12.290	0.000	12.290	10.120	0.011	10.131
	11.050	0.000	11.050	7.450	0.024	7.474

*determined by steady state material balance

Table C.9: Data for the 20°-22 Hydrocyclone at 7 psi with K46 Microbubbles

Inlet Density (g/mL)	wt HDPE UF (g)	wt HDPE OF (g)	wt HDPE* Feed (g)	Wt PP UF (g)	wt PP OF (g)	wt PP* Feed (g)
1.00	0.111	6.061	6.172	0.015	6.052	6.067
	0.116	5.802	5.918	0.007	5.895	5.902
0.93	0.575	7.317	7.892	0.005	5.250	5.255
	0.543	6.851	7.394	0.000	4.923	4.923
0.90	1.749	6.192	7.941	0.076	10.310	10.386
	1.657	5.554	7.211	0.073	10.880	10.953
0.83	8.236	1.761	9.997	2.095	6.572	8.667
	6.621	1.245	7.866	1.673	6.711	8.384
0.75	9.510	0.024	9.534	10.180	0.030	10.210
	7.890	0.013	7.903	9.140	0.028	9.168

*determined by steady state material balance

Table C.10: Data for the 10°-22 Hydrocyclone

Inlet Density (g/mL)	wt HDPE UF (g)	wt HDPE OF (g)	wt HDPE* Feed (g)	Wt PP UF (g)	wt PP OF (g)	wt PP* Feed (g)
1.00	0.107	6.790	6.897	0.008	5.255	5.263
	0.160	5.244	5.404	0.009	5.395	5.404
0.93	1.137	5.502	6.639	0.079	5.998	6.077
	0.947	4.970	5.917	0.122	5.500	5.622
0.91	6.448	4.790	11.238	0.177	7.500	7.677
	2.564	5.190	7.754	0.063	7.240	7.303
0.90	2.500	5.402	7.902	0.138	7.335	7.473
	2.214	4.324	6.538	0.082	6.845	6.927
0.83	8.503	1.507	10.010	void	5.187	void
	7.482	0.996	8.478	1.884	4.920	6.804
0.75	12.910	0.000	12.910	12.683	0.000	12.683
	11.800	0.012	11.812	11.510	0.000	11.510

*determined by steady state material balance

LIST OF REFERENCES

LIST OF REFERENCES

Ali, S.K., Z.C. Yang, J.F. Foss, C.A. Petty, "The Separation Performance of Long Hydrocyclones with an Annular Feed Entry", Paper presented by Syed Ali at the 4th International Conference on Hydrocyclones (September 23-25, 1992).

American Plastics Council, 1993, Post Consumer Plastics Recycling Rate Study - Executive Summary.

American Cyanamid Corp., 1951, "Heavy-Media Separation", *Ceramic Bulletin*, 30(3), 63 (1951).

Altand, B.L., R.M. Enick, E.J. Beckman, and S. Chang, "Optimization of Batch Thermoplastic Microsortation Using Near-Critical Liquids", Paper presented at the 1994 AIChE Annual Meeting, San Fransisco, CA (November 13-18).

Battle K.E., A.P. Moore, J.C. Lynch, and E.B. Nauman, "Plastics Recycling by Selective Dissolution", Transcripts from presentation by Ken Battle at The Dewitt Conference (March 25-27, 1992).

Bradley, D., 1965, The Hydrocyclone, Pergamon Press.

Carlson, D.C. and M. Kakabalia, 1993, "The Use of Hydrocyclone Technology for HDPE Recycling - A Market Study", report from a market survey conducted for the MTA 890 graduate marketing course.

Dahlstrom, D.A.,1949, "Cyclone Operating Factors and Capacities on Coal and Refuse Slurries", *Mining Transactions*, 184, 331 (Sept.).

Dreissen, H.H., and F.J. Fontein, 1963, "Applications of Hydrocyclones and Sieve Bends in Wet Treatment of Coal, Minerals and Mineral Products", *Society of Mining Engineers*, 101 (March).

Dreissen, M.G., 1939, "Cleaning by Heavy Liquids, with Special Reference to the Staatsminjnen-Loess Process", *Journal of The Institute of Fuel*, 329 (August, 1939)

Hegberg B.A., G.R. Brenniman, and W.H. Hallenbeck, 1992, Mixed Plastics Recycling Technology, Noyes Data Corp.

Mark, H.F., & et al., eds., 1985, Encyclopedia of Polymer Science & Engineering, Wiley.

Miller, K.J., M.S. Klima, and R.P. Killmeyer, 1991, "Selection and Production of Dense-Medium Solids for the Micro-Mag Process", Topical Report DOE/PETC/TR-91/5 (DE91011943).

Moder, J. and D.A. Dahlstrom, 1952, "Fine Size, Close Specific Gravity Solids Separation with the Liquid-Solid Cyclone", *Chemical Engineering Progress*, 48(2), 75.

Nugent, D.C., 1991, Process for the Separation and Recovery of Plastics, U.S. Patent (5,022,985).

Perry, R.H., D.W. Green, and J.O. Maloney, eds., 1984, Perry's Chemical Engineers' Handbook, 6th ed., McGraw-Hill Book Company.

Petty, C.A., S.K. Ali, E.A. Grulke, and S.E. Selke, 1993, "Hydrocyclone Classifiers for Microsorting Mixed Thermoplastics from Consumer Waste", Proceedings of Waste Minimization and Utilization of Innovative Concepts - An Experimental Technology Exchange, organized by the U.S. Department of Energy, Austin, TX.

Svarovsky, L., 1984, Hydrocyclones, Holt, Rinehart and Winston Ltd.